The dentition of a new adult Neanderthal individual from Grotte Mandrin, France

Jeanne Fuchs, Antonio García-Tabernero, Antonio Rosas, Hubert Camus, Laure Metz, Ludovic Slimak, Clément Zanolli

Journal of Human Evolution 196 (2024) 103599

Contents lists available at ScienceDirect

Journal of Human Evolution

journal homepage: www.elsevier.com/locate/jhevol

The dentition of a new adult Neanderthal individual from Grotte Mandrin, France

Jeanne Fuchs [a], Antonio García-Tabernero [b], Antonio Rosas [b, c], Hubert Camus [d], Laure Metz [e, f], Ludovic Slimak [g, *], Clément Zanolli [a, *]

[a] Univ. Bordeaux, CNRS, MCC, PACEA, UMR 5199, F-33600 Pessac, France
[b] Department of Paleobiology, National Museum of Natural Sciences, CSIC, Calle Jose Gutierrez Abascal 2, 28006 Madrid, Spain
[c] Area de Antropología Física, Facultad de Ciencias Biológicas y Ambientales, Campus Vegazana s/n, 24071 León, Spain
[d] PROTEE-EXPERT, 4 Rue des Asphodèles, 34750 Villeneuve-lès-Maguelone, France
[e] Aix-Marseille Université, CNRS, Min. Culture, UMR 7269, LAMPEA, Maison Méditerranéenne des Sciences de l'Homme, BP 647, 5 Rue du Château de l'Horloge, F-13094 Aix-en-Provence Cedex 2, France
[f] University of Connecticut, College of Liberal Arts and Sciences, 215 Glenbrook Road, U-4098, Storrs, CT 06269-4098, USA
[g] CNRS, UMR 5288, Centre for Anthropobiology and Genomics of Toulouse, University Toulouse III, Toulouse, France

ARTICLE INFO

Article history:
Received 13 December 2023
Received in revised form
29 August 2024
Accepted 10 September 2024
Available online 2 October 2024

Handling Editor: Dr A Taylor

Keywords:
Homo neanderthalensis
Southeastern France
Late Pleistocene
Dental structure
Distomolars

ABSTRACT

Grotte Mandrin is located in the middle Rhône River Valley, in Mediterranean France, and has yielded 11 Pleistocene archeological and paleoanthropological layers (ranging from the oldest layer J to the youngest layer B) dating from Marine Isotope Stage (MIS) 5 to MIS 3. We report here the nearly complete dentition of an adult Neanderthal individual, nicknamed 'Thorin,' associated to the last phase of the Post-Neronian II, in layer B2 (~44.50–42.25 ka). A previous paleogenetic analysis revealed that Thorin is a male individual and that he shows a deep genetic divergence with other penecontemporaneous Neanderthals from western Europe that possibly occurred ~105 ka. The 31 teeth of Thorin (including two distomolars) are described and analyzed using microcomputed tomography imaging and are compared with other Neanderthals and modern humans. Based on direct observation and measurements on the fossil remains, and using microtomographic imaging, tooth wear, nonmetric characters, crown dimensions, and dental tissue proportions were investigated, and the shape of the enamel–dentine junction of the M^2, M_2, and M_3 was analyzed by geometric morphometrics. Our results indicate that Thorin's teeth show dental characteristics typical of MIS 5–3 Neanderthals. It is also the first time that the presence of two distomolars is reported in a Neanderthal individual, a trait that is rare among modern human populations. Combined with the genetic peculiarities of this individual, the results of the present study imply either a process of morphological convergence among the latest Neanderthal groups or an underestimation of the genetic variability of recent Neanderthal groups.

1. Introduction

1.1. General context

The period between 55 and 40 ka corresponds to major events in Europe in terms of population replacements ending with the disappearance of Neanderthals and the colonization of the continent by modern humans. This process is characterized by the presence of both Middle Paleolithic and early phases of the Upper Paleolithic and the emergence of several 'transitional' technocomplexes distributed across distinct geographical areas (Slimak, 2019). In Western Europe, the Châtelperronian is distributed from Burgundy to Spain (Leroi-Gourhan, 1965; Pelegrin, 1995); the Uluzzian (Palma di Cesnola, 1989) is confined to the Italian and Greek Peninsulas, whereas the Neronian is found only in the Middle Rhône Valley (Slimak, 2004, 2023; Slimak et al., 2022). None of these cultures show any geographical overlap. The historical and cultural complexity of population replacement between Neanderthals and modern humans is not yet fully understood, but it is likely that this process was much longer than previously suspected (Zilhão and d'Errico, 2003; Mellars, 2004; Higham et al., 2014),

* Corresponding authors.
E-mail addresses: ludovic.slimak@cnrs.fr (L. Slimak), clement.zanolli@gmail.com (C. Zanolli).

https://doi.org/10.1016/j.jhevol.2024.103599

extending over a period of at least 10 to 15 millennia, during which modern humans and Neanderthals lived alternately in some of these territories (Slimak, 2023).

The well-differentiated geographical distribution of the cultural groups in western Eurasia from ~55 to 40 ka raises fundamental questions about the dynamics and biocultural aspects that governed the settlement of these populations in these different territories even though the identity of the human groups associated with these different cultural entities remain unclear (Slimak, 2019). Since the middle of the 20th century, it has been commonly believed that the transitional industries represented the last expression of the Neanderthal populations before their extinction (e.g., Leroi-Gourhan, 1965; Pelegrin, 1995), regardless of whether the modern traits characterizing these technical traditions were, according to some, of local origins (d'Errico et al., 1998; Soressi, 2002; Caron et al., 2011) or, for others, acculturations among local populations due to some degree of contact with modern humans (Hublin, 2015; Ruebens et al., 2015). These industries were commonly attributed to the last Neanderthal populations, but since 2010, increasing archeological, paleoanthropological, and genetic evidence indicates that a number of them were made by modern humans (see Slimak, 2023 for a recent review). Recent discoveries indicate that the Uluzzian (Benazzi et al., 2011; Moroni et al., 2018; Oxilia et al., 2022), the Lincombian–Ranisian–Jerzmanowician (Hublin et al., 2023), and the Neronian (Slimak et al., 2022) were in fact produced by modern humans. Another recent study based on trans-Mediterranean comparative analyses concluded that the Châtelperronian could be linked to the northern Early Ahmarian industries and have originated from the eastern Mediterranean region and could thus represent a second wave of modern human colonization of Europe, inducing a full rewriting of the historical replacement models of Neanderthals by *Homo sapiens* populations (Slimak, 2023). This model has since been supported by the discovery of a modern human ilium bone in a Châtelperronian layer at Grotte du Renne, near Arcy-sur-Cure, in northeastern France (Gicqueau et al., 2023). If the technical roots of the Châtelperronian lie in the northern Early Ahmarian from the Levantine region, it would indicate that at least some of the transitional industries could well represent the proxies of various early modern human migrations in Europe (Slimak, 2023). However, the association of Neanderthal remains and Châtelperronian industries at a number of sites, such as in Arcy-sur-Cure (Bailey and Hublin, 2006), suggests that the question of the maker of the Châtelperronian is still not fully resolved.

These complex population dynamics are intimately linked with the cultural, chronological, and geographical overlap between the different hominin groups that lived in Europe ~55 to 40 ka ago. Many archeological sites dated to Marine Isotope Stage (MIS) 3 were excavated decades ago according to the standards of the time, resulting in a loss of information and the accumulation of uncertain, fragile, disputable, or incomplete data or archeological associations (e.g., Semal et al., 2009; Benazzi et al., 2011, 2015; Gravina et al., 2018). Dates are also not always reliable due to contamination or because the period of interest is at the limit of the ^{14}C method (Higham et al., 2014; Devièse et al., 2021). Anthropological data from recent excavations showing rich biocultural associations are extremely rare, and each new specimen discovered in a clear archeological context is of great value and therefore potentially represents a fundamental asset for tackling the true complexity of this 15-millenia period.

1.2. Grotte Mandrin

Grotte Mandrin is located on the eastern bank of the Rhône Valley, near the town of Malataverne, Drôme (Fig. 1A). It is a rock shelter on the slope of the 'Jas des Chèvres' hill at an elevation of 225 m. The cavity exposed to the north spreads 12 m wide, 8 m deep, and 2 m in height (at the maximum level before excavation). The site was discovered in the 1960s by Gaston Etienne, an amateur local archeologist who found late Neolithic and early Bronze Age modern human remains (Allentoft et al., 2022), and reached locally the roof of the Pleistocene layers revealing few lithic artifacts, which were subsequently attributed to the Paleolithic by Jean Combier. A first pit was dug in 1990–1993, and additional excavations revealed six Mousterian layers and a small Proto-aurignacian assemblage. The first excavations of the Pleistocene layers took place from 1993 to 1998 and permitted a first overview of the stratigraphy (Giraud et al., 1998; Slimak, 2008). Since 1999, the excavation has been conducted by Ludovic Slimak, Yves Giraud, Pascal Yvorra, and Laure Metz (Slimak et al., 2024a).

The entire archeological sequence is divided into 11 levels (Fig. 1B), from Level J, dated to MIS 5, to Level B1, dated to MIS 3. The Levels D to B1 encompass the period of the last Neanderthal societies and two of the very first waves of the Upper Paleolithic migrations in Europe (Slimak et al., 2022; Metz et al., 2023; Slimak, 2023). The archeological assemblage is composed of more than ~60,000 lithics for the main pieces but is composed of millions of elements if counting the tiniest flakes coming from the strict sieving of the archeological operations. The paleontological record includes more than ~70,000 faunal remains, as well as a number of human remains (mostly isolated deciduous teeth; Slimak et al., 2022, 2023). The upper sequence (Levels F to B1) documents alternating phases of replacement between Neanderthal occupations (Levels F, D, to B2) and modern human occupations (Levels E and B1). This is attested by the large archeological assemblage associated with human remains in nearly all levels, except in Level B1, the least dense occupation of this Pleistocene sequence attributed to the Protoaurignacian and where no human remains were found (Slimak et al. 2006, 2022, 2023, Metz et al., 2023, 2024a).

1.3. The Neanderthal individual from level B2

In August 2015, several human remains belonging to a single Neanderthal individual (some of them being still skeletally articulated) were discovered in Level B2. Level B2 is the last phase of the Mousterian industry and thus the last Neanderthal reoccupation of Grotte Mandrin after the earliest modern human incursion in Europe in Level E around 54 ka (Slimak et al., 2022).The remains appeared in situ but were highly fragmented and associated with fauna and lithics attributed to the Post-Neronian II (PNII), the very last phase of the Mousterian typically found in the Rhône Valley, in France (Fig. 1C; Slimak, 2023; Slimak et al., 2023, 2024b). This industry is characterized by the production of flakes mainly obtained by discoid flaking, but these technologies are systematically associated with a large range of other technologies including Kombewa, Levallois, and Kostienki technologies or laminar productions, revealing a large set of technical knowledge among these late Neanderthal populations of the PNII (Slimak et al., 2023, 2024b). The PNII blanks are used to produce a large variety of scrapers with a majority of lateral and transversal (commonly straight) scrapers, but the variety of scrapers is very large, and the morphology is particularly diverse, which represents a very classic feature for Neanderthal industries more generally.

The human remains include 31 permanent teeth, a left portion of the lateral palatal process, a fragmentary right hemi-mandible, as well as five adult phalanges with typical Neanderthal features (e.g., ulnar deviation of the pollical distal phalanx and expansion of the distal phalangeal tuberosity; Coqueugniot and Dutour, 2024; Zanolli, 2024; Slimak et al., 2023). The anatomical representation and connections observed during the excavation are compatible with the remains of a single adult Neanderthal individual (Slimak et al., 2023; Zanolli, 2024). Moreover, this individual displays two

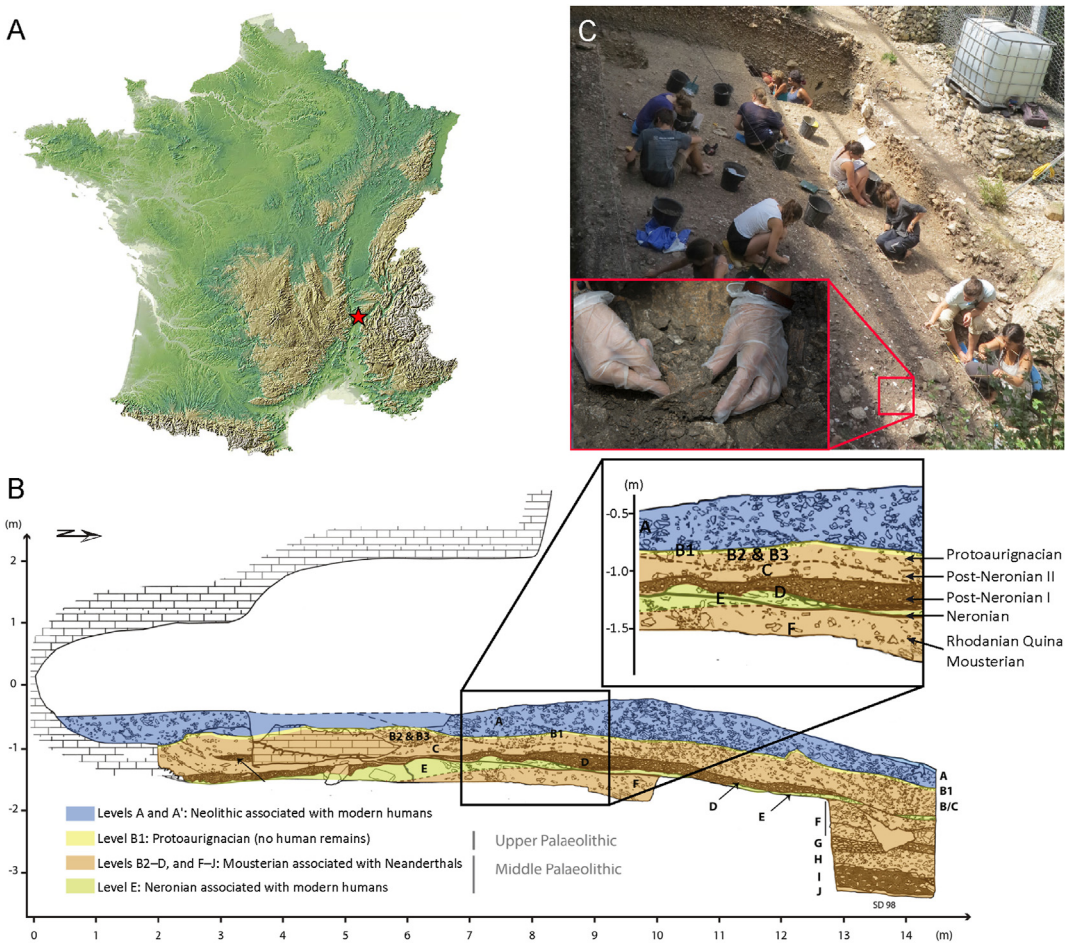

Fig. 1. Map of France with the location of Grotte Mandrin indicated by a red star (A), stratigraphy of the site showing the different geological and archeological levels (B), with an inset highlighting higher level of discrimination between the different levels, and a picture of the site showing the excavation and the area where the various skeletal and dental elements of Thorin were found (red insets; C). (For interpretation of the references to color in this figure legend, the reader is referred to the Web version of this article.)

supernumerary molars, or distomolars. This individual was nicknamed 'Thorin' and because each dental fragment or element was given an independent label, to facilitate reading, this nickname will be used in the following to refer to this individual.

According to the uranium-series age distribution in the fossils, a minimum age of 43.5 ± 4.1 ka can be assigned to Thorin. Combined uranium-series–electron spin resonance modeling yields statistically indistinguishable finite ages of 48 + 5/−13 ka and 49 + 5/−10 ka for Thorin and the Level B2 fauna, respectively (Slimak et al., 2023). Dating of the fossils is in statistical agreement with the general chronostratigraphic position of PNII (~52–42 ka) and its last phase in Level B2 (~44.5–42.25 ka) chronologies. Thorin unambiguously belongs to the Level B2, but its attribution to a specific sublayers of the Level B2 and associated PNII phases is still under evaluation. The recovered body parts appear to be located in a small natural depression (all dental remains were found within a 50-cm^2 square) and could have been deliberately deposited there along the bedrock of a rockshelter (Slimak et al., 2023, 2024c). Following the 2023 field season, it appears very likely that Thorin should be attributed to the very end of the PNII ~44.50–42.25 ka and is thus a late representative of the Neanderthal populations in Europe (Slimak et al., 2024c). However, a recent paleogenetic study conducted on Thorin revealed a deep divergence with other late Neanderthals and long-lasting genetic isolation of this group, with no genetic introgression with other late Neanderthals in Europe (Slimak et al., 2023, 2024c).

In the present study, we describe and investigate the morphology of the dentition of Thorin. More specifically, we aim to document both external and internal structures of the dental tissues using μCT data and to compare this individual with other Neanderthals from a wide chronogeographic range, as well as with modern humans.

2. Materials and methods

2.1. Materials

Thorin A total of 31 permanent teeth are preserved, representing 26 complete teeth (including two M_4s or distomolars) and five incomplete teeth (Table 1). All tooth types are represented, and only the right C^1, right P^3, and right P^4 are missing.

With the aim of studying the morphology of Thorin's teeth and taking into account the genetic results indicating a deep genetic divergence with penecontemporaneous Neanderthal groups (Slimak et al., 2023, 2024c), we divided the Neanderthal comparative samples in two groups, early Neanderthals dating to MIS 7–6 (243–130) and late Neanderthals dating from MIS 5–3 (130–29 ka). Thorin's teeth were compared with those of early Neanderthal (n = 218 for crown metrics and n = 26 for enamel–dentine junction [EDJ] analyses), late Neanderthal (n = 392 and n = 29, respectively), Pleistocene modern human (n = 1109; only for external crown metric comparisons), and

Table 1
List of the dental elements of the Neanderthal individual Thorin.[a]

Accession number	Dental elements
Man16 B2 1267	LI^1
Man15 B2 1700	RI^1
Man16 B2 1268	LI^2
Man15 B2 1800	RI^2
Man16 B2 1239-1240	LC^1
Man16 B2 1238	LP^3
Man16 B2 1260	LP^4
Man19 B2 2920	LM^1
Man15 B2 2001	RM^1
Man16 B2 1256	LM^2
Man15 B2 1900	RM^2
Man16 B2 1254	LM^3
Man15 B2 2000	RM^3
Man19 B2 2581	LI_1, LI_2, RI_1, RI_2, RC_1, RP_3, RP_4, RM_1, RM_2
Man18 B2 1483	LC_1
Man18 B2 1484	LP_3
Man18 B2 1489	LP_4
Man18 B2 1997	LM_1, LM_2
Man16 B2 1258	LM_3
Man19 B2 2898	RM_3
Man16 B2 1270	LM_4
Man19 B2 2897	RM_4

Abbreviations: L = left; R = right.
[a] The accession code is constructed based on the prefix 'Man' for Mandrin, followed by the last two digits of the year of discovery, then by the stratigraphic level in which it was found, and ends with the inventory number.

Holocene modern human samples (n = 587 and n = 39, respectively; Supplementary Online Material [SOM] Tables S1 and S2). The Pleistocene modern human samples date from MIS 5 and 4. The Holocene modern samples are composed of Neolithic, historical periods, and contemporary specimens from Europe and Africa. Comparative data extracted from the literature did not systematically report the individual sample values and composition, preventing us from separating Neanderthals according to their respective chronological grouping. In these cases, we compared Thorin with Neanderthals as a group. For more information on comparative sample composition by analysis, we refer to the sections in the following.

2.2. Microcomputed tomographic scan acquisition and three-dimensional model generation

The teeth of Thorin were scanned by μCT using a GE Sensing Nanotom at the CIRIMAT (UMR 5085, University of Toulouse, France) and a GE Phoenix V/TOME/SX at PLACAMAT (UAR 3626, University of Bordeaux, France) laboratories according to the following parameters: 100–130-kV voltage, 110–250-μA current, 0.1-mm copper filter, and 1200 to 1441 projections over a scan angle of 360°. The final volumes were reconstructed with isotropic voxel sizes of 19.5 to 50.0 μm. The teeth were segmented in Avizo v. 9.2 (ThermoFisher Scientific, Waltham), and three-dimensional (3D) renderings of dental tissues (dentine, enamel, pulp cavity, and cementum) were generated. For the left C^1 and left P^3, the broken roots were virtually reassembled in Avizo with the crown fragments. The surface files of the 31 teeth of Thorin are available online on The Human Fossil Record: A Digital Resource for Research and Education (https://human-fossil-record.org) at the following address: https://human-fossil-record.org/index.php?/category/22801.

2.3. Nonmetric dental traits

A summary of the nonmetric dental features was described in Zanolli (2024), but an independent and extended characterization of the traits is provided here. Occlusal wear was categorized with the method developed by Smith (1984). The description and characterization of the nonmetric traits was divided into three parts: first, at the outer enamel surface (OES); second, at the enamel EDJ; and third, the description of roots and pulp root canals. The dental nonmetric traits, their definition, and wear-scale grades are presented in SOM Table S3. For OES of the crown, we used the Arizona State University Dental Anthropology System developed by Turner et al. (1991) and revised by Scott and Irish (2017). This system has been developed for Holocene modern humans but was also adapted to document dental morphological variability of hominin taxa (Bailey, 2002a, 2002b; Bailey and Lynch, 2005; Bailey and Hublin, 2006, 2013; Martinón-Torres et al., 2012; Irish et al., 2013). In most cases, it is not possible to accurately score the degree of expression of each nonmetric trait due to the advanced wear of Thorin's teeth. We thus recorded the dental traits either as present, absent, or unobservable. In cases of uncertainties regarding the stage of a trait, we added a question mark to indicate that it is probably a minimum estimate. With the aim of assessing additional nonmetric traits, we have scored morphological features at the EDJ following previously established protocols (Skinner et al., 2008; Bailey et al., 2011; Martínez de Pinillos et al., 2014; Martinón-Torres et al., 2014; Ortiz et al., 2012, 2018; Martin et al., 2017; Davies et al., 2021).

2.4. Dental crown size

All the dental variables were measured on the 3D surface generated with the constrained smoothing algorithm in Avizo. The buccolingual (BL) and mesiodistal (MD) tooth crown diameters were measured in mm as the maximum distance between the mesial and distal side and the buccal and lingual side, respectively, along the principal axes of the crown. Only the BL diameter was measured for the anterior teeth because of the advanced occlusal wear affecting mesial and distal aspects of the crown. Adjusted Z-scores were used to compare Thorin's measurements with the means and standard deviations of the comparative samples (Maureille et al., 2001; Scolan et al., 2012). This method based on the Student's t inverse distribution enables the comparison of unbalanced samples, which is often the case when dealing with the fossil record. The formula is as follows: $[(x - m)/(SD \times \sqrt{(1 + 1/n)})/(\text{Student.t.inverse}(0.05; n - 1)]$, where x is the value of the variable, m is the mean of the same variable for a comparative sample, n is the size of the comparative sample for this variable, and SD is the standard deviation of the comparative sample for this variable. When Z-scores fall between −1 and +1, the measure is included within 95% of the variation of the comparative group and is thus considered as statistically compatible with the comparative range of variation. Adjusted Z-scores were generated for both BL and MD. The comparative samples are detailed in SOM Table S1.

2.5. Tooth root size

To measure root dimensions, the teeth were virtually separated into the crown and root parts using the cervical plane (SOM Fig. S1). For anterior teeth, the cervical plane was defined following the Le Cabec et al. (2013) protocol as the plane passing by the greatest curvature on the lingual and buccal surfaces. For molars and premolars, to place the cervical plane, we first created a best-fit plane passing through the cervix following the method described by Olejniczak et al. (2008). We then moved this plane upward in the crown to reach the position of the first complete ring of the enamel. Finally, the plane halfway between the last points of enamel and the first complete ring of enamel was defined as the reference plane. Furthermore, to separate the root stem and root branch in molars, a bifurcation plane was positioned following the protocol of Kupczik and Hublin (2010). Intraobserver and interobserver tests

were conducted to assure that the separation planes were correctly positioned for the different measurements, resulting in <0.05% difference in all cases.

The following variables were measured for all teeth: root length (RtL) in mm, root surface area (RtA) in mm^2, and root volume (RtV) including dentine, pulp, and cementum volumes in mm^3. We also computed the adjusted Z-scores (Maureille et al., 2001; Scolan et al., 2012) for all of these variables (RtL, RtA, and RtV) to statistically assess if the roots of Thorin's teeth are statistically compatible with the variation of the comparative groups. As explained in Section 2.4, whenever adjusted Z-scores range between −1 and +1, the variable is included within 95% of the variation of the comparative group and is thus considered statistically compatible with the latter.

All comparative data were extracted from the literature (Kupczik and Hublin, 2010; Le Cabec et al., 2013; Kupczik et al., 2019; Pan et al., 2019). For molars, only Thorin's mandibular molars were investigated as no method and comparative material for maxillary molars are readily available in the literature.

2.6. Lower molar root proportions and volumetric bifurcation index

The bifurcation plane is parallel to the cervical plane passing through the center of the inter-radicular surface (SOM Fig. S2). The following variables were measured only for mandibular molars: total volume of stem root in mm^3 (Vstem) between the cervical plane area and the bifurcation plane, and total volume of branch root mm^3 (Vbranch) between the bifurcation plane and apex. For mandibular molars, the volume of bifurcation index (VBF; in percentage) was computed as follows: VBF = Vstem/(Vstem + Vbranch). We also computed the adjusted Z-scores (Maureille et al., 2001; Scolan et al., 2012) for all of these variables (Vstem, Vbranch, and VBF) to statistically assess if the roots of Thorin's teeth are compatible with the variation of the comparative groups. When Z-scores range between −1 and +1, the variable is included within 95% of the variation of the comparative group and is thus considered statistically compatible with the latter.

All comparative data were extracted from the literature (Kupczik and Hublin, 2010; Kupczik et al., 2019).

2.7. Geometric morphometric analyses of the enamel–dentine junction

A previous study has demonstrated that the EDJ shape is effective in distinguishing between earlier (pre-Eemian to Eemian) and later (after 115 ka) Neanderthals (Martin et al., 2017), so we divided Neanderthals into two groups, those dating to MIS 7–6 and those from MIS 5–3 (SOM Table S2).

Geometric morphometric analyses of the EDJ were conducted only for the better-preserved molars, namely M^2s, right M_2, and M_3s. In each of the investigated molars, some dentine crests and/or horns were slightly affected by occlusal wear and reconstructions were made following the geometric method described in Zanolli et al. (2018). The reconstructed EDJs are shown in SOM Figure S3. In the maxillary molars, fives curves of 15–25 semilandmarks were placed along the EDJ ridges between the four primary dentine horns (SOM Fig. S4). In the mandibular molars, four curves of 15–25 semilandmarks were placed along the EDJ ridges between the four primary dentine horns (SOM Fig. S4). Principal component analyses and canonical variate analyses (CVAs) were computed for each molar position. The molars of Thorin were projected a posteriori into the CVA morphospaces. We also computed the cross-validated CVA and confirmed that group discrimination is not spurious (Cardini and Polly, 2020). Posterior probabilities based on CVA were calculated for each molar of Thorin.

All statistical analysis and plots were computed in R v. 4.2.3 (R Core Team, 2023) using the packages 'Morpho' v.2.11. (Schlager, 2023), 'rgl,' and 'MASS.'

3. Results

Based on the position and orientation of the interproximal contact facets on the tooth crowns, we virtually reconstructed the jaw of Thorin (Fig. 2), showing that the two distomolars (M_4s) are impacting the distal aspect of the M_3s. A description of the main dental morphological features of the 31 teeth of Thorin is provided in the following, and the virtual renderings of the teeth are shown in Figs. 3–8.

3.1. Nonmetric dental traits

Maxillary incisors I^1 and I^2 exhibit an advanced degree of occlusal wear (stage 5). There are marked interproximal facets on the mesial and distal surfaces of all incisors. The I^1s and I^2s differ in a few traits: the crown of the I^1s is more symmetric and labiolingually compressed, whereas that of the I^2s is mesiodistally smaller and more asymmetric. The root of the I^1s is also straighter, whereas that of the I^2s exhibits a more curved labial aspect and a distally tilted root apex. On the I^1s, two slightly developed crests remain visible on the lingual aspect, suggesting that a shoveling morphology was originally present (left I^1: stage 2?; right I^1: stage 2/3; Fig. 9B). Moreover, some digitations visible at the base of the lingual aspect of the I^1 crown indicate the presence of a tuberculum dentale, even though the degree of development cannot be scored (Fig. 9A). At the OES of the I^2, a deep fossa is visible on the lingual surface associated with two marginal crests, indicative of a marked shoveling (left I^2: stage 4?; right I^2: stage 5?; Fig. 9A). A marked degree of labial curvature is visible in the occlusal view on both I^1 and I^2 (stage 4; Fig. 9A and B). The shovel-shape morphology and labial curvature are also observable on the EDJ of the incisors, as well as three digitations at the base of the lingual aspect of the I^2 (Fig. 9A and B).

All incisors display a single root (with a single pulp canal), with a shallow longitudinal depression on the mesial surface and a smooth distal surface (Fig. 3). There is a thick deposit of cementum in the apical third of the roots of both I^1s and left I^2, whereas on the right I^2, cementum is deposited all along the root.

Maxillary canine Only the left C^1 is preserved, and it displays an advanced degree of occlusal wear (stage 6). Interproximal contact facets are visible on the mesial and distal surfaces. Due to occlusal wear, no dental traits can be described at the OES or EDJ, but a faint groove at the base of the lingual aspect could be indicative of the former presence of a tuberculum dentale (Fig. 9C).

The root is single (with a single pulp canal), with a longitudinal depression on the mesial surface and a shallower one the distal aspect (Fig. 3). An apposition of cementum is present in the apical half of the root, and in the distolingual aspect, there is a localized excess of cementum.

Maxillary premolars Only the left P^3 and P^4 are preserved. They display an advanced degree of occlusal wear (stage 5), and there are marked interproximal contact facets on the mesial and distal surfaces of the crown. Due to occlusal wear, no dental traits can be described at the OES or EDJ.

The left P^3 root is fractured into two parts but shows two fused branches, with a marked longitudinal depression on mesial and distal surfaces (Fig. 4). The left P^4 root (that was fractured into two parts and reassembled) bifurcates around the middle of the root. The root pulp canal is double in both the left P^3 and P^4. A layer of cementum covers the apical half of the root in both premolars (Fig. 4).

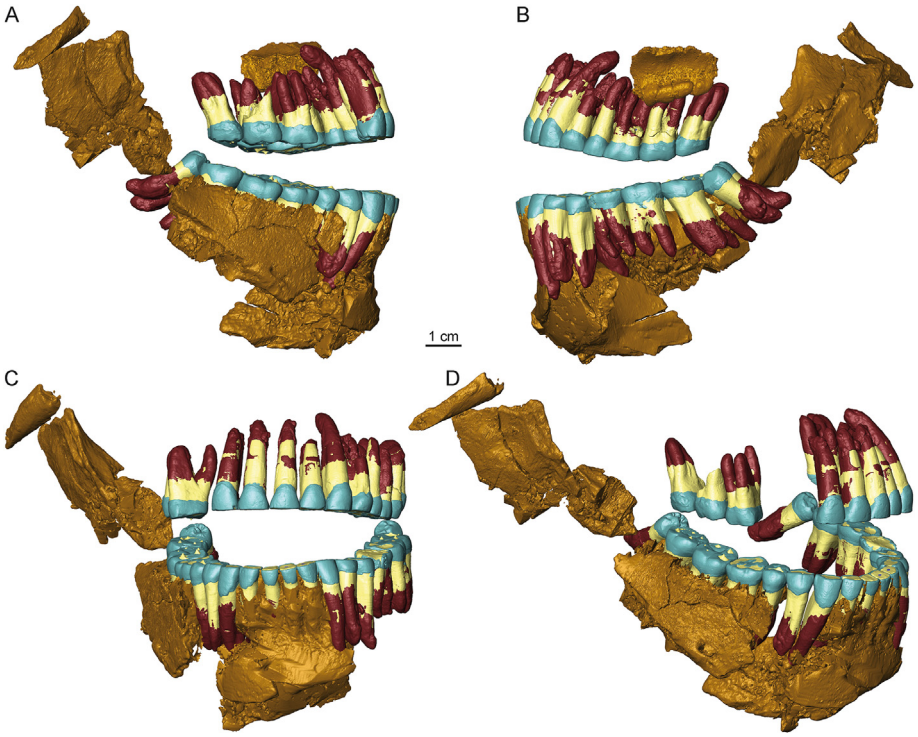

Fig. 2. Virtual reconstruction of the jaw of Thorin in right (A), left (B), anterior (C), and anterolateral (D) views. The jaw includes all the bone fragments recovered until 2023 and all the dental elements virtually reassembled and aligned along the arcade based on the position and orientation of the interproximal contact facets between the teeth. (For interpretation of the references to color in this figure, the reader is referred to the Web version of this article.)

Maxillary molars The M^1s display advanced occlusal wear (stage 4), whereas M^2s and M^3s are relatively less worn (M^2s: stage 3; M^3s: stage 3 or 4). The interproximal contact facets of the M^1s and M^2s are well developed. In the M^3s, an interproximal wear facet is visible on the mesial aspect of the crown, and a large and inclined facet is present on the distolingual aspect of the crown. At the OES, the metacone is visible in all maxillary molars, and the hypocone is well developed in the M^1s and M^2s (stage 4; Fig. 9D), present in the right M^3, and unobservable on the left M^3. At the EDJ, the metacone is moderately developed for the M^1s, M^2s, and right M^3 and is faint for the left M^3 (Fig. 9D). The hypocone is large for the M^1s, moderate for the M^2s and right M^3, and unobservable for the left M^3. The metaconule is unobservable for the left M^1 and M^3s, absent in the right M^1 (stage 0), and faint in the M^2s (stage 1 or 2; Fig. 9E). A groove forms the Carabelli's trait on the M^1s, M^2s, and left M^3 (stage 1), and for the right M^3, a pit is present in this position (stage 2; Fig. 9D). On the distal marginal crest of the paracone, the presence/absence of a postparacone tubercle is unobservable in both M^1s, but a minor expression can be seen on the M^2s and M^3s (stage 2; Fig. 9E). The crista obliqua is unobservable in the left M^1 and left M^3, whereas it is well expressed in the right M^1 and M^2s (stages 2 and 3; Fig. 9D).

On the left M^1, only the mesiobuccal root is completely preserved and connected to the crown, whereas the lingual and distobuccal roots are broken in the first third of the root. The right M^1 preserves all root branches, showing one lingual root and two buccal roots. For both M^2s, the root is broken a few millimeters below the crown, but the remnant suggests that a lingual and two buccal branches were originally present (Fig. 5). The left M^3 has a lingual branch and two fused buccal branches. In the right M^3, the lingual root is broken in the cervical third of the root, and a buccal root is preserved with three fused branches (two mesially located and one in the distal position). The pulp chambers of the M^1s and M^2s show four and three pulp horns, respectively, and they all have three pulp canals (Fig. 5). The M^3s show only two pulp horns on the chamber and four pulp chambers (two being partly fused at the apex of the right M^3). There is a cementum layer covering the apical half to apical third of the root of all molars.

Mandibular incisors Both I_1 and I_2 present an advanced degree of occlusal wear (stage 6), and there are marked interproximal contact facets on the mesial and distal surfaces of the crown. Due to the advanced occlusal wear, it is not possible to detect any nonmetric trait either at the OES of incisor or at the EDJ of the I_1. A short portion of the distal marginal crests is still observable at the EDJ surface of the I_2.

The incisors all show a single root (with a single pulp canal along most of the root, bifurcating into two thin canals at the apex) and display a shallow longitudinal depression on the distal surfaces and a smooth mesial surface (Fig. 6). There is a cementum apposition in the apical third of the root of all mandibular incisors.

Mandibular canines The C_1s display an advanced degree of occlusal wear (stage 5), and there are interproximal facets on the mesial and distal surfaces. Due to occlusal wear, no dental trait can be described at the OES. The lower part of the marginal crests is observable at the EDJ and indicates that both mesial and distal accessory crests were present. In both C_1s, the lower part of the distal accessory ridges is observable (Fig. 6).

Both C_1s show a single root (with a single pulp canal in the left C_1 and a bifid canal toward the apex of the right C_1) and display a smooth mesial surface and a shallow longitudinal depression along the distal aspect.

Mandibular premolars The premolars exhibit moderate to advanced occlusal wear (P_3s and left P_4: stage 4; Zanolli, 2024; right P_4: stage 3), and interproximal facets are present in the mesial and distal surfaces. In the occlusal view, the P_3 and P_4 crowns are asymmetric (Fig. 7). Between the protoconid and the metaconid, there is a transverse crest on the right P_3 and P_4, visible at both the OES and EDJ levels (Fig. 10A), but this trait is unobservable for the left P_3 and P_4.

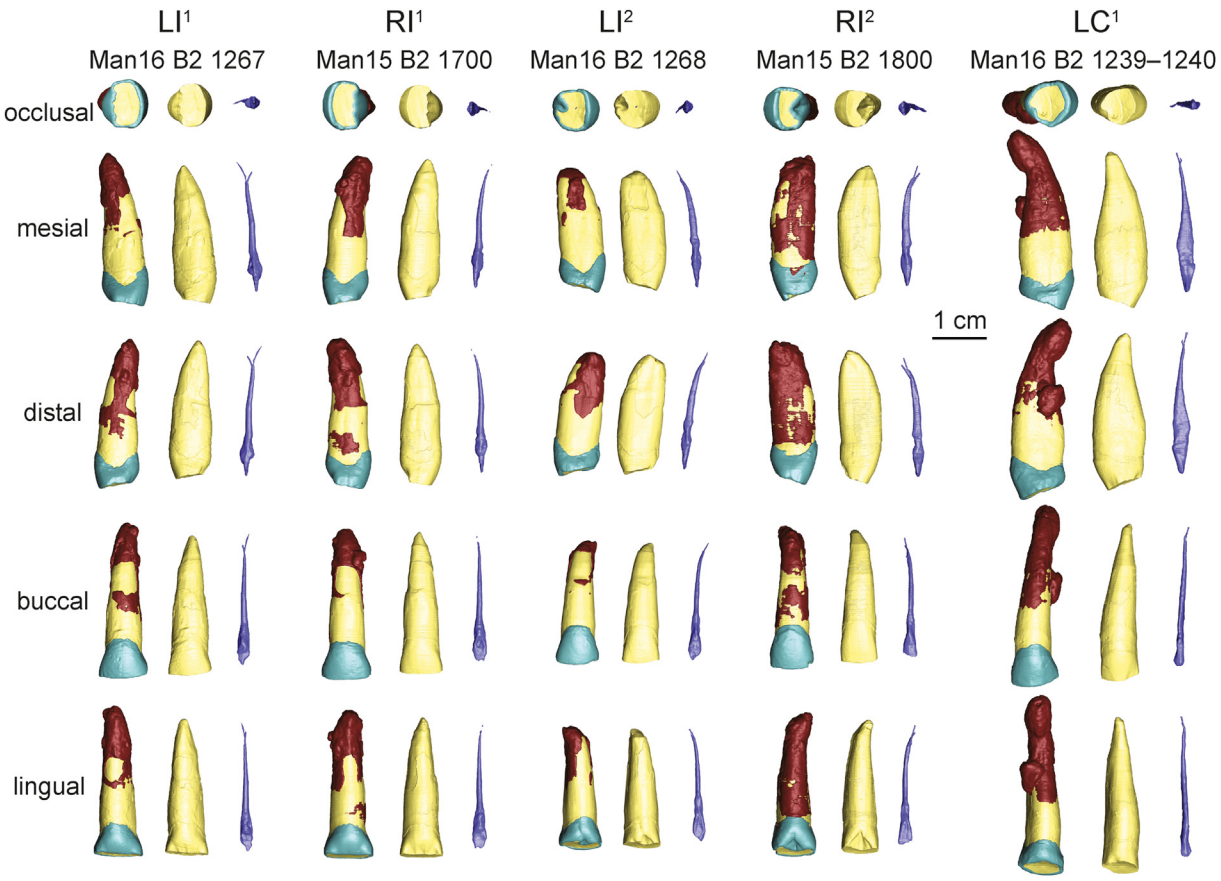

Fig. 3. Virtual renderings of the maxillary anterior teeth of Thorin. For each tooth, the external morphology with enamel in blue, dentine in yellow, and cementum in red (left column), dentine (middle column), and pulp (right column) are illustrated in different anatomical views. Abbreviations: L = left; R = right. (For interpretation of the references to color in this figure legend, the reader is referred to the Web version of this article.)

The left P_3 and both P_4s show a single root, with a marked longitudinal depression on the mesial and distal surfaces. The right P_3 root is divided into three fused branches, one lingual branch, and two buccal branches (Tome's root). There is a single pulp canal in the left P_3 and both P_4s (even though it is bifid at the apical extremity in the left P_3) and a double one along most of the right P_3 root branches (the buccal canal being bifid at the apex). There is a deposit of cementum on half of the root of all premolars (Fig. 7).

Mandibular molars The left M_1 displays advanced occlusal wear (stage 6), whereas the right M_1 exhibits a marked, but less advanced, occlusal wear (stage 4). The right M_2 is moderately worn (stage 3), and the left M_2 exhibits a slightly more advanced occlusal wear (stage 4). Both M_3s are moderately worn (stage 3 or 4). There are marked interproximal mesial and distal contact facets in M_1s, M_2s, and M_3s. There is no occlusal wear on M_4s, but a large wear facet affects the mesial and mesio-occlusal aspects, suggesting that both distomolars impacted the M_3 crowns (Fig. 2). At the OES, only a few dental traits are observable on the molars. A developed hypoconulid is detectable on the right M_2 despite the occlusal wear, and a hypoconulid and the trigonid crest are still perceptible on the left M_2 and on M_3s (Fig. 10B), but they are unobservable for both M_1s. In all mandibular molars, the protostylid is absent at the OES (stage 0; even though presence/absence in the M_1s is difficult to evaluate because of the occlusal wear). Due to occlusal wear, no nonmetric traits are observable on either the OES or EDJ surfaces of the left M_1. At the OES, the hypoconulid of the right M_1 and left M_2 appears to be larger than that on the right M_2 and on both M_3s. No accessory distal or lateral cusps are observable on the left M_2 at either the OES or EDJ levels. The left M_3 shows no accessory cusp on the OES or EDJ (stage 0). A small distal accessory cusp (interconulid type) is visible on the EDJ of the right M_2 (stage 1, single) and right M_3 (stage 1, triple; Fig. 10C). No lateral accessory cusp is visible at the OES or EDJ levels of the right M_2 (stage 0), whereas a small interconulid-type accessory cusp is present on the right M_3 (stage 1, single). On the right M_1, a mid-trigonid trigonid is present at the EDJ, but its expression is not scorable due to occlusal wear. A continuous mid-trigonid crest is present in the right M_2 and on both M_3s, perceptible at the OES, but well-expressed at the EDJ (Fig. 10B). In all molars where this feature is preserved, the mid-trigonid crest height dips in the middle (stage 2) and is positioned as a middle segment (stage 1). At the EDJ of the right M_1 an uninterrupted talonid crest between the distal trigonid crest running down from the protoconid and the talonid crest running from the entoconid is perceptible. On the right M_2 and right M_3, an interrupted talonid crest is visible on the EDJ (stage 3; Fig. 10B). Due to advanced occlusal wear, this trait is not observable for the left M_2. In most molars, the anterior fovea is only visible on the EDJ, except for the right M_3, on which this feature is also preserved at the OES. It is large in the right M_2, and in both M_3s (stage 4), and is smaller (but not scorable) in the right M_1 and left M_2 (Fig. 10B). The crown of the M_4s is mesiodistally compressed and shows marginal crests, as well as a small fossa on the distobuccal aspect of the crown (Fig. 8). On the right M_4, an interrupted crest is present between the metaconid and the protoconid. The EDJ of the M_4s exhibits a centrally placed dentine horn, and, similar to the OES, three fossae are observable. In the right M_4, there is an uninterrupted crest between

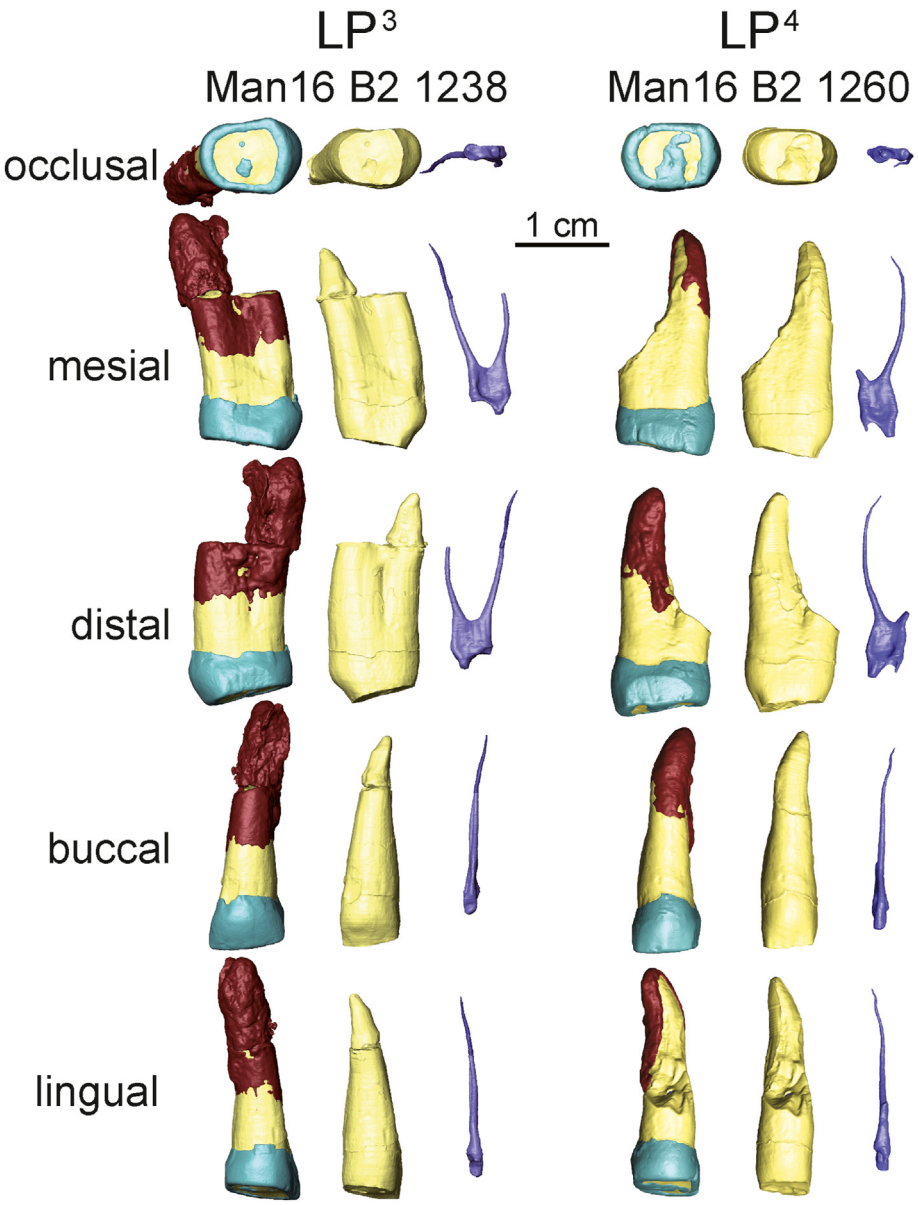

Fig. 4. Virtual renderings of the maxillary premolars of Thorin. For each tooth, the external morphology with enamel in blue, dentine in yellow, and cementum in red (left column), dentine (middle column), and pulp (right column) are illustrated in different anatomical views. The accession number is indicated above each tooth (cf. Table 1). Abbreviation: L = left. (For interpretation of the references to color in this figure legend, the reader is referred to the Web version of this article.)

the metaconid and the protoconid. Multiple accessory dentine horns corresponding to minute accessory cusps can also be detected on the EDJ of the distomolars (the EDJ of the right M_4 shows more accessory cusps and crests than the left M_4; Fig. 8). Due to the unusual morphology of both M_4s, and the absence of distomolars in the fossil record, we cannot compare them with other specimens, but we provide here in the following various dimensions of the crown and root.

The measurements of the left M_4 are as follows: BL = 8.8 mm; MD = 7.6 mm; RtL = 18.18 mm; RtA = 654.6 mm^2; RtV = 431.09 mm^3.

The measurements of right M_4 are as follows: BL = 9.4 mm; MD = 7.6 mm; RtL = 18.56 mm; RtA = 689.41 mm^2; RtV = 443.67 mm^3.

The M_1s, M_2s, and right M_3s have a mesial root with two fused branches and a distal root. The left M_3 root is divided into three branches: one mesial and two fused distal branches. The M_1s, M_2s, and right M_3 display two mesial pulp canals and a single distal canal, whereas the left M_3 has two mesial pulp canals (fused at the apex) and a single distal pulp canal. Both M_4s show a single root with a single pulp canal.

3.2. Tooth crown diameters

Maxillary anterior teeth On average, early Neanderthals exhibit larger BL diameters than late Neanderthals and Pleistocene and Holocene modern humans, even if all Pleistocene groups overlap (Table 2). The BL diameter of Thorin's maxillary anterior teeth is smaller than that of early and late Neanderthal means but exceeds that of Pleistocene and Holocene modern human means. The BL diameter of Thorin's maxillary anterior teeth exceed the range of Holocene modern humans, but they overlap with those of the early and late Neanderthals and Pleistocene modern humans, except for I^1s that are below the range of the early Neanderthals.

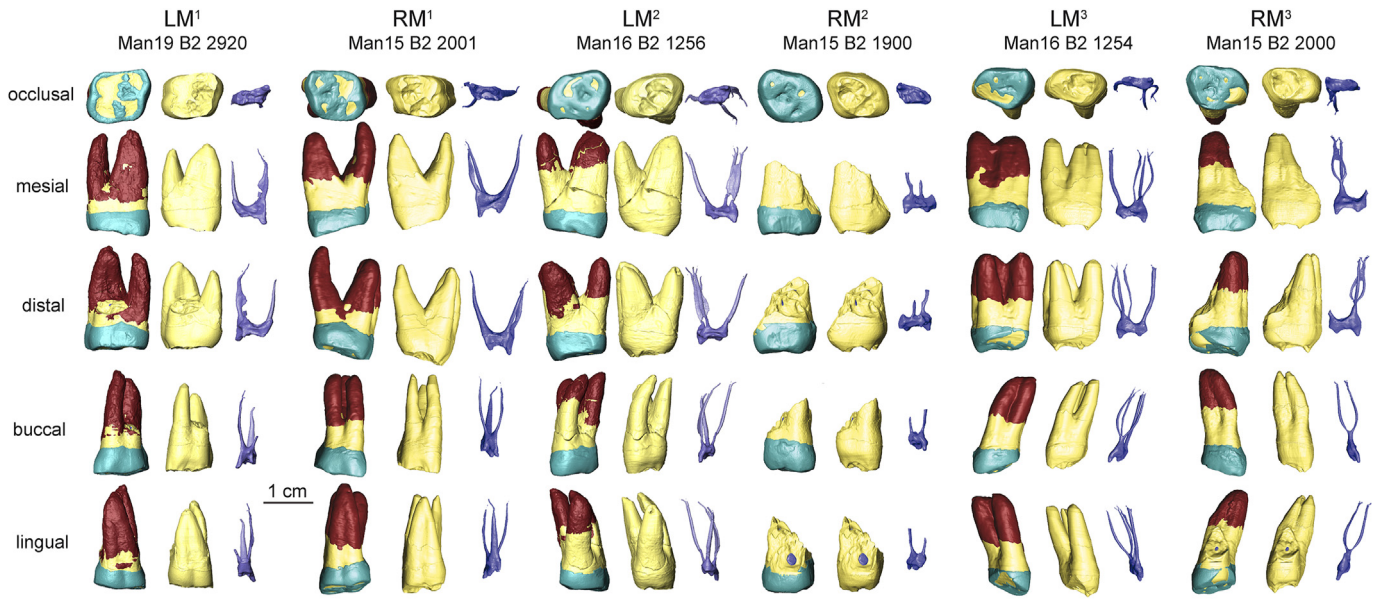

Fig. 5. Virtual renderings of the maxillary molars of Thorin. For each tooth, the external morphology with enamel in blue, dentine in yellow, and cementum in red (left column), dentine (middle column), and pulp (right column) are illustrated in different anatomical views. The accession number is indicated above each tooth (cf. Table 1). Abbreviations: L = left; R = right. (For interpretation of the references to color in this figure legend, the reader is referred to the Web version of this article.)

The adjusted Z-score analysis shows that BL dimensions of all Thorin's anterior teeth fall within 95% of variation of early and late Neanderthals and Pleistocene modern humans but statistically exceeds the range of Holocene modern humans (Fig. 11).

Maxillary premolars On average, early Neanderthals have higher BL and MD diameters than late Neanderthals and Pleistocene and Holocene modern humans (Table 2). Early Neanderthal values overlap with the ranges of late Neanderthals and Pleistocene

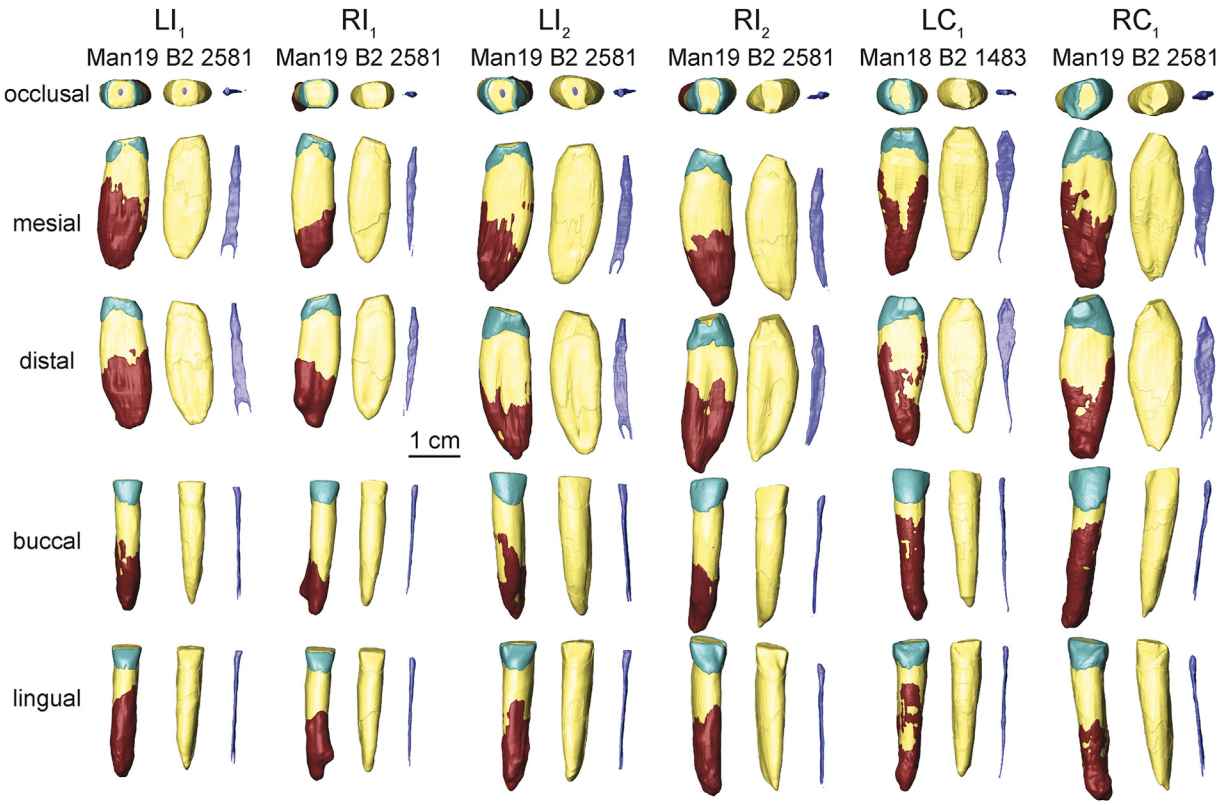

Fig. 6. Virtual renderings of the mandibular anterior teeth of Thorin. For each tooth, the external morphology with enamel in blue, dentine in yellow, and cementum in red (left column), dentine (middle column), and pulp (right column) are illustrated in different anatomical views. The accession number is indicated above each tooth (cf. Table 1). Abbreviations: L = left; R = right. (For interpretation of the references to color in this figure legend, the reader is referred to the Web version of this article.)

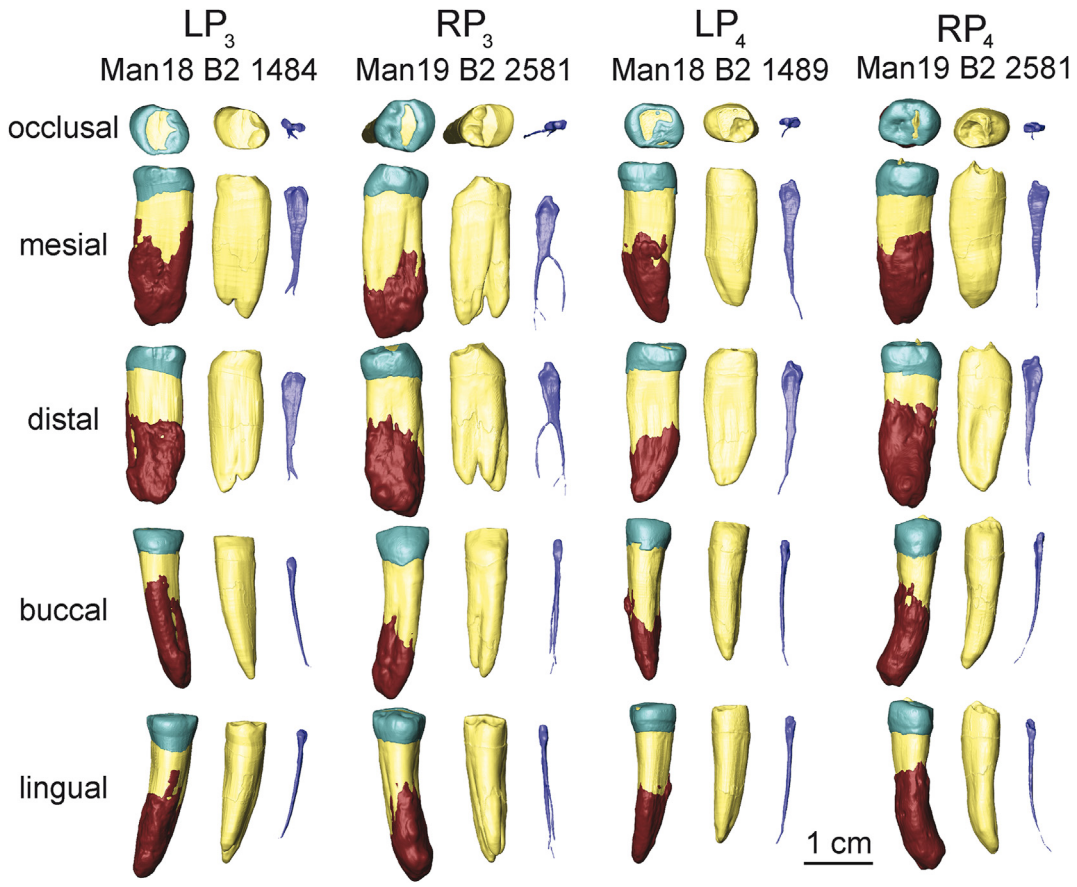

Fig. 7. Virtual renderings of the mandibular premolars of Thorin. For each tooth, the external morphology with enamel in blue, dentine in yellow, and cementum in red (left column), dentine (middle column), and pulp (right column) are illustrated in different anatomical views. The accession number is indicated above each tooth (cf. Table 1). Abbreviations: L = left; R = right. (For interpretation of the references to color in this figure legend, the reader is referred to the Web version of this article.)

modern humans and exceed those of Holocene modern humans. Thorin's premolars show smaller dimensions than the early Neanderthal average condition, but they are close to the means of late Neanderthals and are larger than the means of Pleistocene and Holocene modern humans. The BL and MD diameters of the left P_3 and P_4 of Thorin are compatible with the early (except for the MD diameter of the LP^4 that falls below) and late Neanderthal and Pleistocene modern human ranges, but they exceed that of Holocene modern humans.

The adjusted Z-scores of the BL and MD diameters lie within 95% of the variation of the early and late Neanderthal and Pleistocene modern human samples and are statistically larger than those of Holocene modern humans (Fig. 11).

Maxillary molars Early Neanderthals have higher BL and MD diameters on average than late Neanderthals and Pleistocene and Holocene modern humans, even if they overlap with the ranges of the other groups (Table 2). The BL and MD diameters of all maxillary molars of Thorin are smaller than the early and late Neanderthals means but higher than the means of Pleistocene and Holocene modern humans. The BL diameters of the M^1s, M^2s, and M^3s of Thorin fall in the range of the four groups. The MD diameter of the M^1s and M^3s falls in the range of late Neanderthals and Pleistocene and Holocene modern humans but is smaller than the minimal value of the early Neanderthals range. The MD diameter of the M^2s exceeds the range of Holocene modern humans and falls in the range of the three other groups.

The adjusted Z-scores of the BL and MD diameters of Thorin M1s are not only statistically closest to the late Neanderthal and Pleistocene modern human conditions but are also statistically within the range of early Neanderthals and Holocene modern humans (even if at the extreme limit of variation of these two groups). Thorin M^2 and M^3 crown diameters fall within the range of variation of early and late Neanderthals and Pleistocene and Holocene modern humans (Fig. 11); only the MD diameter of Thorin's M^2s statistically exceeds the 95% range of variation of Holocene modern humans.

Mandibular anterior teeth Early Neanderthals have larger BL dimensions on average than late Neanderthals and Pleistocene and Holocene modern humans (Table 2). Early Neanderthal values overlap with the range of late Neanderthals and Pleistocene modern humans and exceed those of Holocene modern humans. The mandibular anterior teeth of Thorin are close to the means of the late Neanderthals and overlap with the range of the early and late Neanderthals and Pleistocene modern humans, but they exceed the range of the Holocene modern humans.

The adjusted Z-scores of the BL diameters of Thorin mandibular anterior teeth statistically fall within 95% of the variation of early and late Neanderthals and Pleistocene modern humans and beyond the 95% range of variation of Holocene modern humans (Fig. 11).

Mandibular premolars Early Neanderthals exhibit the largest BL and MD diameters on average compared with late Neanderthals and Pleistocene and Holocene modern humans even if all comparative groups overlap (Table 2). Crown diameters of the P_3s and P_4s of Thorin are smaller on average than those of early Neanderthals and slightly exceed the mean of late Neanderthals, whereas they are larger than the means of Pleistocene and

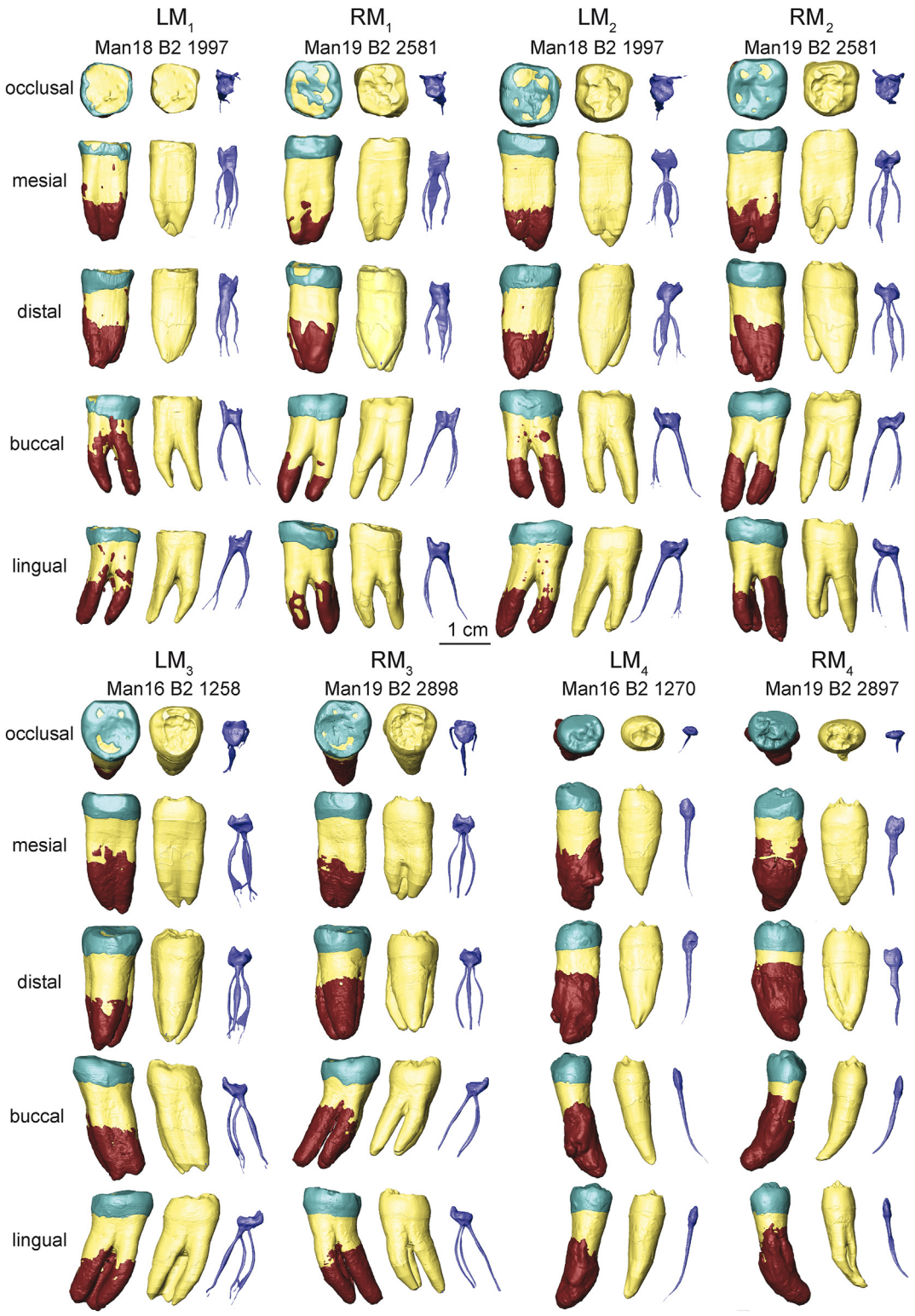

Fig. 8. Virtual renderings of the mandibular molars of Thorin. For each tooth, the external morphology with enamel in blue, dentine in yellow, and cementum in red (left column), dentine (middle column), and pulp (right column) are illustrated in different anatomical views. The accession number is indicated above each tooth (cf. Table 1). Abbreviations: L = left; R = right. (For interpretation of the references to color in this figure legend, the reader is referred to the Web version of this article.)

Holocene modern humans. Both BL and MD diameters of Thorin premolars are included in the range of early and late Neanderthals and Pleistocene modern humans, as well as within the upper range of Holocene modern humans.

The adjusted Z-scores of the BL and MD diameters of Thorin's P_3 and P_4 fall within 95% of the variation of early and late Neanderthals and Pleistocene modern humans. The MD of Thorin premolars is compatible with the range of variation of Holocene humans, but the

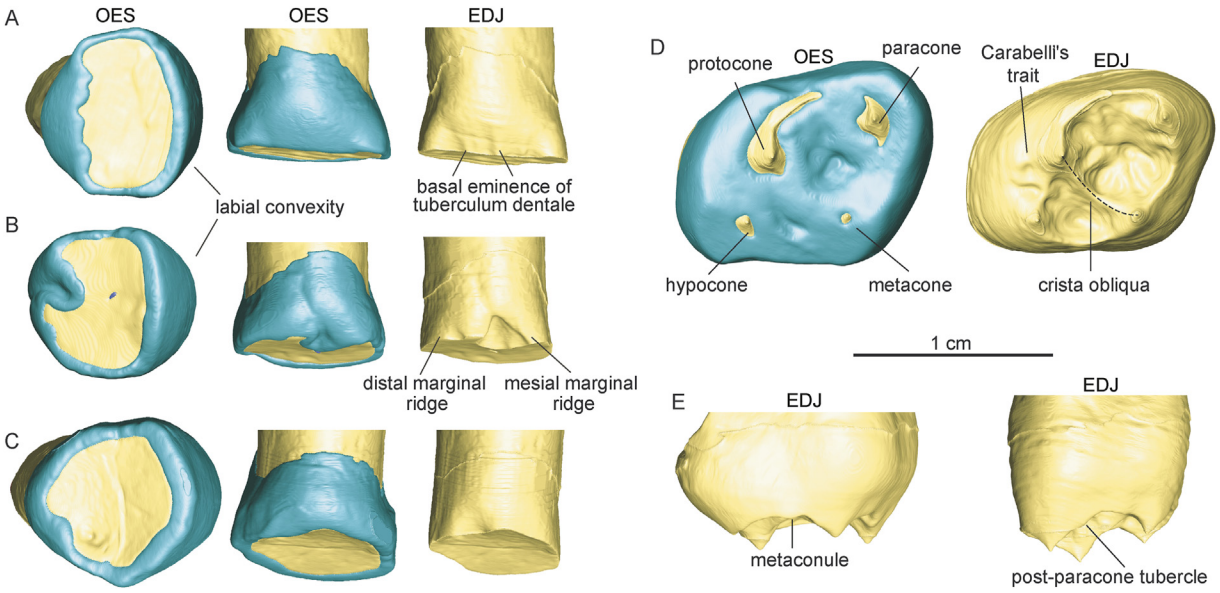

Fig. 9. Dental nonmetric traits at the outer enamel surface (OES) and enamel–dentine junction (EDJ) of the left I^1 (A), I^2 (B), and C^1 (C) in occlusal and lingual views and of the left M^2 in occlusal (D) and mesial and lingual views (E). (For interpretation of the references to color in this figure, the reader is referred to the Web version of this article.)

BL diameter is statistically larger than that of Holocene modern humans (Fig. 11).

Mandibular molars Early Neanderthals have larger BL and MD diameters on average than late Neanderthals and Pleistocene and Holocene modern humans, but all comparative groups largely overlap (Table 2). The mandibular molars of Thorin are smaller than the mean of the early Neanderthals, close to the average condition of late Neanderthals mean, and larger than the means of Pleistocene and Holocene modern humans. The right M_1, M_2s, and M_3s of Thorin fall in the range of the four comparative groups (except for the BL diameter of the M_3s).

The adjusted Z-scores of BL and MD diameters of Thorin's M_1s, M_2s, and M_3s fall within 95% of the variation of the four comparative groups, except for the BL diameter of the right M_1 that falls

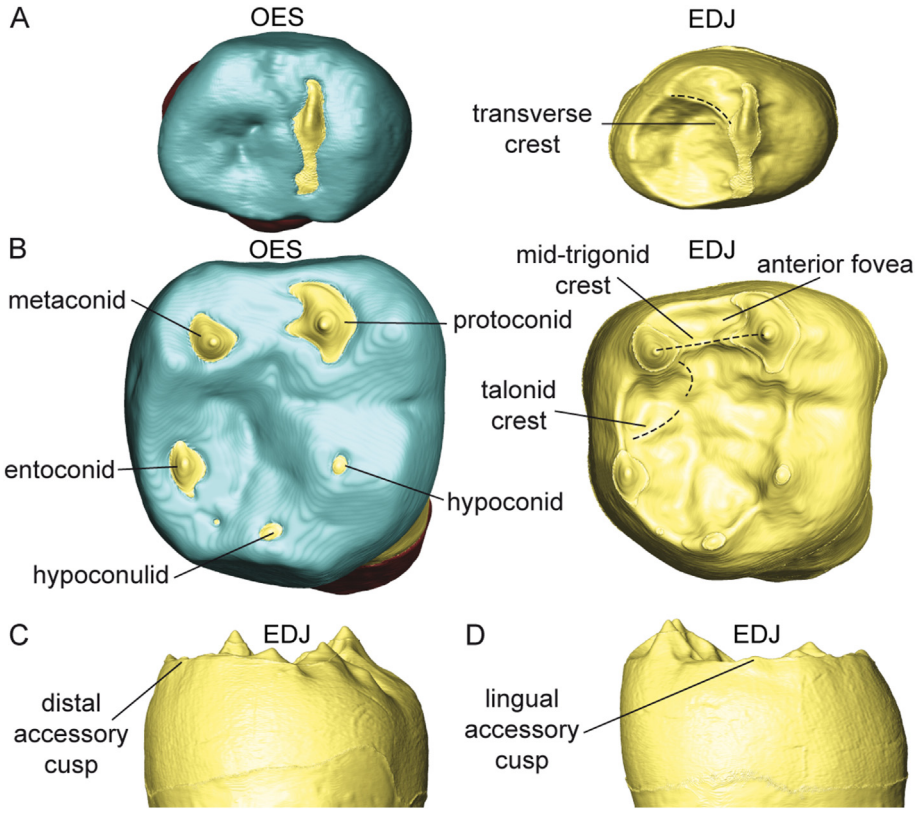

Fig. 10. Dental nonmetric traits at the outer enamel surface (OES) and enamel–dentine junction (EDJ) of the right P_4 in the occlusal view (A) and of the right M_2 in occlusal, (B), distal (C), and lingual views (D). (For interpretation of the references to color in this figure, the reader is referred to the Web version of this article.)

Table 2
Buccolingual (BL) and mesiodistal (MD) diameters of the teeth of Thorin compared with those of early Neanderthals (ENEAs), late Neanderthals (LNEAs), Pleistocene modern humans (PMHs), and Holocene modern humans (HMHs).

Specimen/group		I^1	I^2	C^1	P^3		P^4		M^1		M^2		M^3	
		BL	BL	BL	MD	BL	MD	BL	MD	BL	MD	BL	MD	BL
Man16 B2 1267 L		8.2												
Man15 B2 1700 R		8.2												
Man16 B2 1268 L			7.9											
Man15 B2 1800 R			7.9											
Man16 B2 1239-1240 L				9.6										
Man16 B2 1238 L					8	10.3								
Man16 B2 1260 L							7.6	10.2						
Man19 B2 2920 L									11.1	11.8				
Man15 B2 2001 R									11.0	12.1				
Man16 B2 1256 L											11.4	12.7		
Man15 B2 1900 R											11.4	12.8		
Man16 B2 1254 L													9.6	12.6
Man15 B2 2000 R													9.5	12.6
ENEA	Mean	9.0	8.8	10.2	8.6	11.4	8.1	10.7	12.6	12.9	11.1	12.9	10.4	12.3
	SD	0.5	0.6	0.7	0.5	0.5	0.6	0.6	0.7	0.8	1.0	0.7	0.7	0.6
	Range	8.1–9.7	7.8 9.9	8.9–11.4	8.2–9.3	10.3–12.2	6.8–8.7	9.7–11.4	11.9–13.6	12.1–14.2	10.0–13.1	12.0–14.2	9.8–11.4	11.7–13.5
	n	12	17	17	9	9	10	10	10	10	10	10	7	7
LNEA	Mean	8.3	8.3	9.7	7.4	10.4	7.0	10.2	10.8	12.2	10.5	12.4	9.3	11.9
	SD	0.4	0.6	0.5	0.6	0.7	0.6	0.4	0.7	0.5	0.7	1.1	0.8	1.3
	Range	7.8–9.3	6.5–9.0	8.4–10.5	6.2–8.4	7.8–11.5	6.1–8.0	9.3–11.1	9.3–12.5	11.1–13.4	9.1–11.8	9.7–14.5	6.8–10.6	7.7–14.2
	n	17	19	22	26	26	17	17	20	20	22	22	21	21
PMH	Mean	7.7	7.0	9.1	7.3	9.8	7.0	9.8	10.7	12.2	10.2	12.3	9.0	11.6
	SD	0.5	0.5	0.7	0.6	0.7	0.8	0.7	0.7	0.6	0.8	0.8	1.4	1.1
	Range	6.3–8.7	5.9–8.1	7.7–10.7	6.0–8.4	8.6–11.6	5.9–12.3	7.6–11.5	8.4–12.7	9.2–13.5	8.9–12.6	10.3–14.0	7.0–11.6	6.9–13.5
	n	29	45	71	72	72	75	75	98	98	92	92	69	69
HMH	Mean	7.2	6.4	8.2	6.7	8.8	6.4	9.0	10.0	11.3	9.2	11.3	8.5	10.9
	SD	0.4	0.4	0.7	0.4	0.5	0.4	0.5	0.5	0.6	0.7	0.8	0.8	1.0
	Range	6.5–7.8	5.4–7.4	7.1–9.4	7.9–9.8	7.9–9.8	5.5–7.5	8.1–9.9	8.4–11.4	10.2–12.5	7.8–10.5	9.9–13.9	7.3–10.5	9.3–13.2
	n	20	34	42	43	43	42	42	42	42	41	41	30	30

Specimen/group		I_1	I_2	C_1	P_3		P_4		M_1		M_2		M_3	
		BL	BL	BL	MD	BL	MD	BL	MD	BL	MD	BL	MD	BL
Man19 B2 2581 L		7.3												
Man19 B2 2581 R		7.0												
Man19 B2 2581 L			7.4											
Man19 B2 2581 R			7.6											
Man18 B2 1483 L				9.2										
Man19 B2 2581 R				8.8										
Man18 B2 1484 L					7.7	9.3								
Man19 B2 2581 R					7.4	9.2								
Man18 B2 1489 L							7.6	9.4						
Man19 B2 2581 R							7.6	9.6						
Man18 B2 1997 L											11.2	10.5		
Man19 B2 2581 R									10.4	10.6	11.7	11.3		
Man16 B2 1258 L													12.1	11.4
Man19 B2 2898 R													11.1	11.5
ENEA	Mean	7.7	8.1	9.4	8.3	9.3	8.2	9.8	12.4	11.4	12.5	11.5	12.2	10.8
	SD	0.4	0.4	0.5	0.5	0.6	0.7	0.8	0.6	0.7	1.1	0.7	0.7	0.5
	Range	6.9–8.2	7.3–8.8	8.7–10.3	7.3–9.2	8.3–10.3	6.9–9.4	8.8–11.7	11.4–13.6	10.3–12.9	10.0–14.0	9.8–12.5	11.2–13.9	9.8–11.4
	n	11	10	14	12	12	16	16	16	16	17	17	13	13
LNEA	Mean	7.3	7.9	8.8	7.3	8.9	7.2	9.0	11.0	10.7	11.2	10.8	11.6	10.9
	SD	0.5	0.6	0.8	0.5	0.7	0.6	0.6	1.3	0.5	1.0	0.7	0.9	0.8
	Range	6.4–8.8	6.8–9.0	7.0–10.3	6.1–8.2	7.3–9.9	5.9–8.4	7.2–10.0	7.0–12.6	9.5–11.6	8.3–12.7	9.2–12.3	7.6–12.8	8.4–12.4

(*continued on next page*)

Table 2 (*continued*)

Specimen/group		I_1	I_2	C_1	P_3		P_4		M_1		M_2		M_3	
		BL	BL	BL	MD	BL	MD	BL	MD	BL	MD	BL	MD	BL
	n	18	21	37	29	29	28	28	31	31	35	35	29	29
PMH	Mean	6.5	7.0	8.5	7.2	8.4	7.3	8.8	11.7	11.1	11.1	10.9	11.1	10.8
	SD	0.4	0.5	0.8	0.7	0.6	0.6	0.6	0.9	0.7	0.9	0.8	1.1	0.7
	Range	5.5–7.3	5.9–8.1	6.7–10.0	6.0–9.7	7.0–10.2	5.7–9.5	7.7–10.9	9.8–14.7	8.3–12.8	9.2–13.1	8.2–13.0	9.0–13.1	9.7–12.9
	n	35	49	70	70	70	72	72	87	87	87	87	64	64
HMH	Mean	6.0	6.4	7.7	6.7	7.6	6.9	8.1	10.9	10.2	10.4	10.0	10.5	9.7
	SD	0.4	0.4	0.5	0.5	0.6	0.4	0.6	0.6	0.6	0.7	0.6	0.8	0.8
	Range	5.1–6.8	5.4–7.2	6.8–8.5	5.5–8.1	6.6–9.0	6.1–7.7	7.0–9.6	9.4–12.1	9.1–11.2	8.9–11.8	8.9–11.4	9.0–12.6	7.9–11.3
	n	31	38	29	42	42	43	43	33	33	42	42	36	36

Abbreviations: L = left; R = right; SD = standard deviation.
The accession code is constructed based on the prefix 'Man' for Mandrin, followed by the last two digits of the year of discovery, then by the stratigraphic level in which it was found, and ends with the inventory number.

beyond the 95% of the variation of the earlier Neanderthals and for the BL diameter of M_3s that statistically exceeds the Holocene modern human range (Fig. 11).

3.3. Root size

Maxillary anterior teeth Neanderthals have the highest RtL, RtA, and RtV values on average in comparison to Pleistocene and Holocene modern humans (Table 3). The I^1s, I^2s, and left C^1 of Thorin show RtL, RtA, and RtV values that are closest to the Neanderthal mean and generally exceed the range of variation of Pleistocene and Holocene modern humans.

The adjusted Z-scores of the three variables (RtL, RtA, and RtV) for the three anterior teeth of Thorin are statistically included in the 95% of the variation range of Neanderthals but exceed that of Pleistocene and modern human (Fig. 12).

Mandibular anterior teeth Neanderthals have higher RtL, RtA, RtV on average than Pleistocene and Holocene modern humans. The lower limit of the Neanderthal range overlaps with the upper limit of the Pleistocene modern human range, but it exceeds the Holocene modern human range (Table 3). Thorin's left I_1 RtL value is higher than the Neanderthal mean, but RtA is lower. However, Thorin's left I_1 shows higher RtV in comparison with the Neanderthal mean, and even exceeds the Neanderthal range. The right I_1, I_2s, and C_1 display higher RtL, RtA, and RtV values than the average Neanderthal condition, but are included in the upper limit of the Neanderthal range (except for RtA of the I_2s and RtV of the right I_2).

The adjusted Z-scores for the three variables (RtL, RtA, and RtV) of Thorin's I_1s, I_2s, and C_1 fall within 95% of the variation of Neanderthals (except for RtV of the left I_1, which exceeds the range of all comparative groups), and statistically exceed the Pleistocene and Holocene modern human ranges (Fig. 12).

Mandibular premolars Neanderthals have the highest mean values for RtL, RtA, and RtV in comparison with Holocene modern humans (Table 3). Thorin's P_3s and P_4s display higher RtL, RtA, and RtV values than the Neanderthal mean and exceed the range of this group. For all of Thorin's premolars, RtL, RtA, and RtV values exceed the range of variation of Holocene modern humans.

The adjusted Z-scores for RtL of Thorin's left P_3 and RtA of the left P_4, as well as RtV of the left P_3 and P_4, fall within 95% of the variation of the Neanderthal sample, but all other variables are statistically outside the variation of both Neanderthals and Holocene modern humans (Fig. 12).

Mandibular molars Earlier Neanderthals have on average higher RtL, RtA, and RtV values than later Neanderthals Pleistocene and Holocene modern humans, even if all groups overlap for RtL, RtA, and RtV values for each molar position, but exceed the Holocene modern human range (Table 3). Thorin's molars display similarly high or even higher RtL, RtA, and RtV values than the early and late Neanderthal means. Thorin molar roots are included within the early Neanderthal range for M_1s, and are at the higher end or exceed the range of this group for M_2s and M_3s, and are generally higher than the values of late Neanderthals, even if they are at the superior extreme of variation for RtV. The RtL, RtA, and RtV values of Thorin's molars are greater than the means of Pleistocene and Holocene modern humans, partly overlapping with the Pleistocene modern human range and exceeding the Holocene modern human range.

The adjusted Z-scores of RtL computed for Thorin's M_1s, M_2s, and M_3s fall within 95% of the variation of the early and late Neanderthal and Pleistocene modern human samples but statistically exceed the Holocene human condition (Fig. 12). The RtA values of the M_3s statistically exceed those of all four comparative groups, whereas for the other molar positions, Thorin falls within 95% of the variation of the Pleistocene groups but systematically exceeds

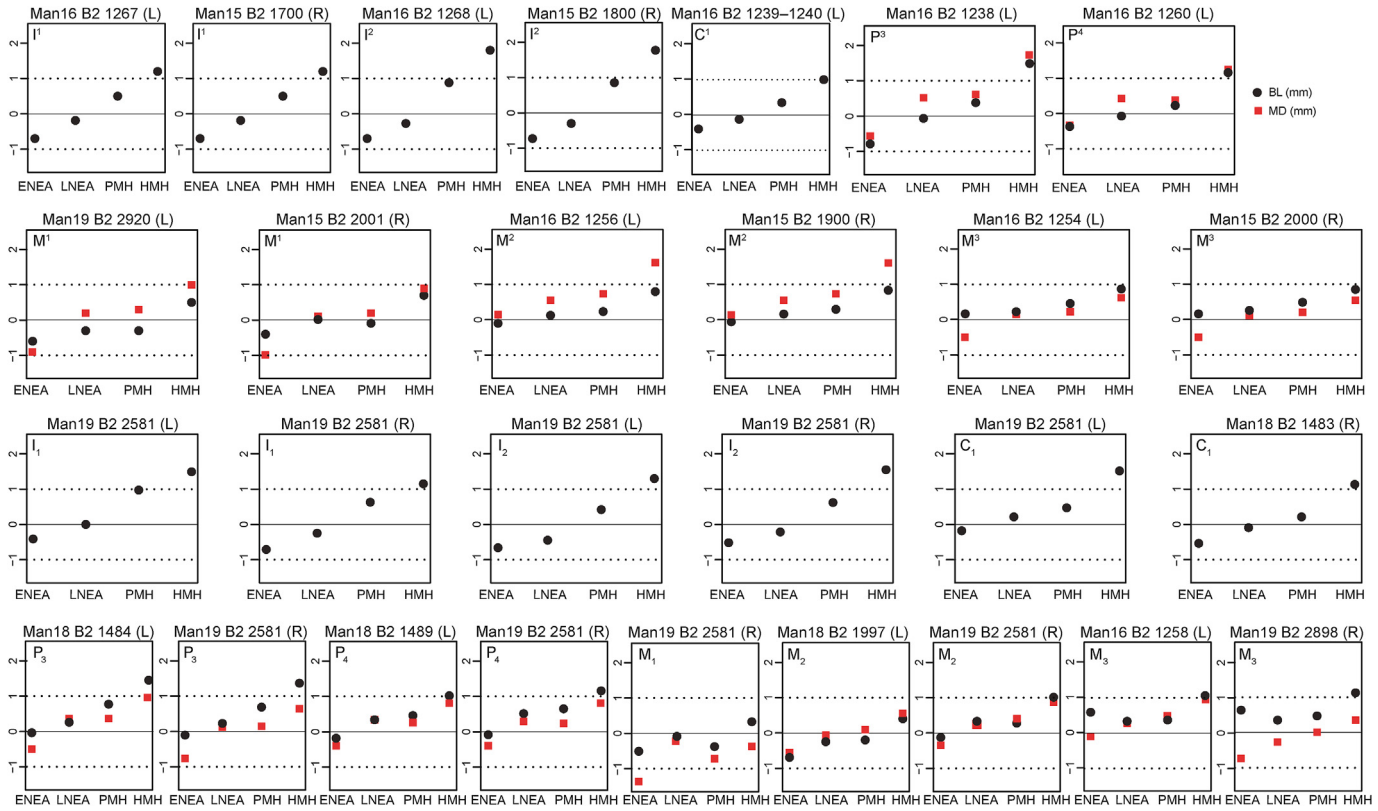

Fig. 11. Adjusted Z-score plots of buccolingual (BL; black circles) and mesiodistal (MD; red squares) diameters of Thorin teeth compared to the variation of early Neanderthal (ENEA), late Neanderthal (LNEA), Pleistocene modern human (PMH), and Holocene modern human (HMH) samples. The solid line passing through 0 represents the mean, and the dotted lines passing through −1.0 and +1.0 represent the 95% limit of the variation of the comparative groups. The accession number of each tooth is indicated above their respective plot (cf. Table 1) Abbreviations: L = left; R = right. (For interpretation of the references to color in this figure legend, the reader is referred to the Web version of this article.)

the Holocene human range (Fig. 12). For M_1s and M_2s, RtV values are within the range of early and late Neanderthals, and of Pleistocene modern humans, exceeding the modern human condition. For M_3s, Thorin is only statistically compatible with early and late Neanderthals and exceeds the range of Pleistocene and Holocene modern humans.

3.4. Molar root proportions and volumetric bifurcation index

Early Neanderthals have the highest Vstem and VBF values and the smallest Vbranch values on average in comparison with late Neanderthals and Pleistocene and Holocene modern humans (Table 4). The Vstem values of Thorin's molars are within the early and late Neanderthal ranges and are within with the upper limits of the Pleistocene and Holocene modern humans ranges (or slightly exceed them). Thorin's mandibular molars have on average higher Vbranch values than early and late Neanderthals and Pleistocene and Holocene modern humans, with those of the M_1s being within the upper limit of the early and late Neanderthal ranges, whereas those of M_2s and M_3s exceed the ranges of the three groups. Thorin's molars display smaller VBF than the early and late Neanderthal means, and they are within the lower limit of the Neanderthal range for this variable.

The adjusted Z-scores of Vstem of all mandibular positions of Thorin are included within 95% of the variation of the early and late Neanderthal and Pleistocene modern human ranges but exceed those of Holocene modern humans (except for M_2s; Fig. 13). For the adjusted Z-scores of Vbranch, the M_1s of Thorin are statistically included in the 95% range of variation of all groups (the right M_1 being at the extreme limit), whereas for M_2s, Thorin is only statistically within the range of late Neanderthals and Pleistocene modern humans, and only the left M_3 is within the range of one of the groups (Pleistocene modern humans). The adjusted Z-scores of VBF fall in 95% of the variation of the four comparative groups for all mandibular molar positions, except the right M_3, which exceeds the range of late Neanderthals (the right M_1 being at the extreme limit of early Neanderthals; Fig. 13).

3.5. Geometric morphometric analyses of the enamel–dentine junction

For the geometric morphometric analyses of the EDJ of Thorin's M^2s, right M_2, and M_3s, comparisons were made with earlier and later Neanderthals and Holocene modern humans. The three groups are discriminated in the analyses, with the two Neanderthal groups overlapping partially among them, but Neanderthals and modern humans being well discriminated (Fig. 14; Table 5). In the CVA plot of the M^2s, there is a slight overlap between the three comparative groups. Late Neanderthals tend to have a more developed hypocone that is placed more distolingually than in the early Neanderthals, whereas the Holocene modern humans display a proportionally large trigon basin and a small trigon with a reduced hypocone (Fig. 14A). The M^2s of Thorin fall in the late Neanderthal range, even though they are also close to the early Neanderthal specimen D165 from Krapina. The cross-validated CVA classifies the M^2s of Thorin as a late Neandertal, with a posterior probability of 82% for the left M^2 and 60% for the right M^2 (Table 5). For M_2s, there is a clear separation between the three comparative

Table 3
Root length (RtL; in mm), root surface area (RtA; in mm^2), and root volume (RtV; in mm^3) of the teeth of Thorin compared with early Neanderthals (ENEAs), late Neanderthals (LNEAs), Neanderthals (NEAs; whenever ENEA and LNEA could not be separated), Pleistocene modern humans (PMHs), and Holocene modern humans (HMHs).[a]

Specimen/group		I^1			I^2			C^1		
		RtL	RtA	RtV	RtL	RtA	RtV	RtL	RtA	RtV
Man16 B2 1267 L		20.83	371.28	479.58						
Man15 B2 1700 R		20.13	392.93	525.98						
Man16 B2 1268 L					16.05	345.32	437.18			
Man15 B2 1800 R					18.79	329.27	519.17			
Man16 B2 1239-1240 L								26.63	596.13	881.65
NEA	Mean	17.23	315.31	452.00	17.62	343.08	487.24	22.51	454.30	650.57
	SD	2.40	60.66	123.52	1.85	42.87	90.99	2.48	60.28	98.94
	Range	10.54–19.79	162.90–409.32	195.84–693.61	14.69–19.97	252.79–409.22	310.68–633.22	17.69–25.16	311.23–539.41	406.87–817.26
	n	17	17	17	18	18	18	12	12	12
PMH	Mean	13.50	220.25	274.95	13.70	188.35	193.01	16.90	287.24	343.56
	SD	2.09	38.50	47.14	1.82	33.39	47.14	2.09	43.89	73.63
	Range	10.61–15.80	166.18–276.11	197.44–384.88	10.78–15.81	155.52–241.54	193.01–137.87	12.55–19.57	216.30–342.31	229.55–459.33
	n	6	6	6	6	6	6	8	8	8
HMH	Mean	12.94	192.33	225.60	12.98	172.11	172.22	16.07	254.20	308.10
	SD	1.41	30.43	46.60	1.41	28.01	39.65	1.43	37.79	71.25
	Range	10.08–16.32	142.58–262.53	147.75–333.03	10.06–16.27	109.00–224.88	94.10–256.16	13.53–18.71	200.85–318.76	213.56–423.88
	n	24	24	24	22	22	22	12	12	12

Specimen/group		I_1			I_2			C_1		
		RtL	RtA	RtV	RtL	RtA	RtV	RtL	RtA	RtV
Man19 B2 2581 L		19.15	366.67	468.92	20.03	383.04	488.54	23.88	540.27	821.78
Man19 B2 2581 R		19.39	350.96	424.89	20.94	403.73	532.59			
Man18 B2 1483 L								24.88	503.03	734.41
NEA	Mean	17.19	300.66	330.34	18.42	335.93	396.22	20.71	412.37	602.33
	SD	1.93	43.38	62.15	2.03	50.58	77.40	2.95	97.14	152.63
	Range	13.18–20.86	195.57–358.86	200.08–421.73	14.81–21.63	240.21–403.59	258.89–507.60	16.05–25.64	221.80–619.68	339.49–902.34
	n	17	17	17	15	15	15	16	16	16
PMH	Mean	12.74	168.19	145.42	14.73	199.10	180.07	15.92	258.27	295.5
	SD	0.84	17.4	21.53	1.03	20.82	25.66	1.74	25.76	41.94
	Range	11.84–14.20	152.13–203.05	121.21–182.69	13.31–16.17	180.57–263.90	149.23–232.89	13.45–18.88	215.69–307.67	208.71–373.61
	n	9	9	9	10	10	10	10	10	10
HMH	Mean	12.67	154.29	127.49	14.09	185.83	165.99	16.55	271.32	327.07
	SD	1.45	23.61	26.18	1.42	26.15	32.34	1.80	53.55	93.48
	Range	10.12–16.66	115.34–200.65	75.48–193.28	10.73–18.41	129.79–241.58	101.63–260.60	13.18–19.22	158.08–387.71	181.58–572.45
	n	39	39	39	47	47	47	23	23	23

Specimen/group		P_3			P_4		
		RtL	RtA	RtV	RtL	RtA	RtV
Man18 B2 1484 L		18.89	445.87	625.52			
Man19 B2 2581 R		20.97	504.02	698.16	21.46	469.69	709.96
Man18 B2 1489 L					21.18	428.89	571.55
NEA	Mean	17.98	327.92	413.28	16.93	330.04	417.25
	SD	0.86	40.07	102.65	1.01	43.64	72.36
	range	16.11–18.76	260.64–386.01	276.38–526.87	15.74–18.51	261.09–391.20	325.13–531.79
	n	8	8	8	8	8	8
HMH	Mean	15.38	261.56	293.52	15.94	267.71	313.18
	SD	1.33	47.85	57.91	1.12	25.71	59.32
	Range	13.00–17.11	206.66–355.04	229.30–383.31	14.20–17.41	224.20–300.98	216.93–389.37
	n	8	8	8	9	9	9

Specimen/group	M_1			M_2			M_3		
	RtL	RtA	RtV	RtL	RtA	RtV	RtL	RtA	RtV
Man18 B2 1997 L	15.70	593.91	761.01	17.62	686.57	981.04			
Man19 B2 2581 R	16.51	620.31	891.04	18.53	795.07	1137.7			
Man16 B2 1258 L							17.29	639.41	1000.80

Table 3 (*continued*)

Specimen/ group		M_1			M_2			M_3		
		RtL	RtA	RtV	RtL	RtA	RtV	RtL	RtA	RtV
Man19 B2 2898 R								18.23	744.53	1043.40
ENEA	Mean	16.19	598.87	795.98	16.37	524.38	828.20	16.27	494.53	798.61
	SD	1.57	87.30	176.06	2.53	73.50	215.05	2.35	47.02	166.82
	Range	14.23–18.45	464.98–691.67	507.28–999.90	12.04–19.88	408.29–609.31	541.65–1090.74	13.04–18.93	411.77–545.39	584.86–1043.01
	n	9	9	9	8	8	8	8	8	8
LNEA	Mean	14.86	510.30	691.58	16.07	550.93	813.38	16.33	455.91	722.85
	SD	1.20	60.43	140.36	1.34	91.68	142.83	1.99	53.14	183.73
	Range	13.33–17.00	427.29–575.00	513.92–882.12	14.10–17.63	377.87–639.53	584.23–994.18	14.47–18.88	398.16–553.57	566.66–1071.11
	n	8	8	8	6	6	6	6	6	6
PMH	Mean	15.20	584.78	762.75	16.30	562.43	799.36	15.30	458.46	639.02
	SD	1.64	106.64	180.23	1.56	115.40	175.42	1.62	73.29	107.09
	Range	12.88–17.67	404.32–722.72	449.97–1008.74	13.43–18.30	429.50–735.30	532.53–978.17	13.10–18.30	364.18–548.39	457.42–741.91
	n	11	11	11	9	9	9	8	8	8
HMH	Mean	13.69	424.62	485.02	13.99	397.32	464.55	12.49	322.33	380.02
	SD	0.94	65.58	104.04	1.74	88.11	118.18	1.82	122.05	150.80
	Range	11.88–14.73	314.25–505.24	340.37–682.30	10.82–16.81	273.57–571.55	349.95–730.55	9.87–16.06	176.70–516.96	218.59–655.50
	n	12	12	12	16	16	16	8	8	8

Abbreviations: L = left; R = right; SD = standard deviation.
The accession code is constructed based on the prefix 'Man' for Mandrin, followed by the last two digits of the year of discovery, then by the stratigraphic level in which it was found, and ends with the inventory number.
[a] Comparative data extracted from Le Cabec et al. (2013) for the anterior teeth, from Pan et al. (2019) for the mandibular premolars, and from Kupczik and Hublin (2010) and Kupczik et al. (2019) for the mandibular molars.

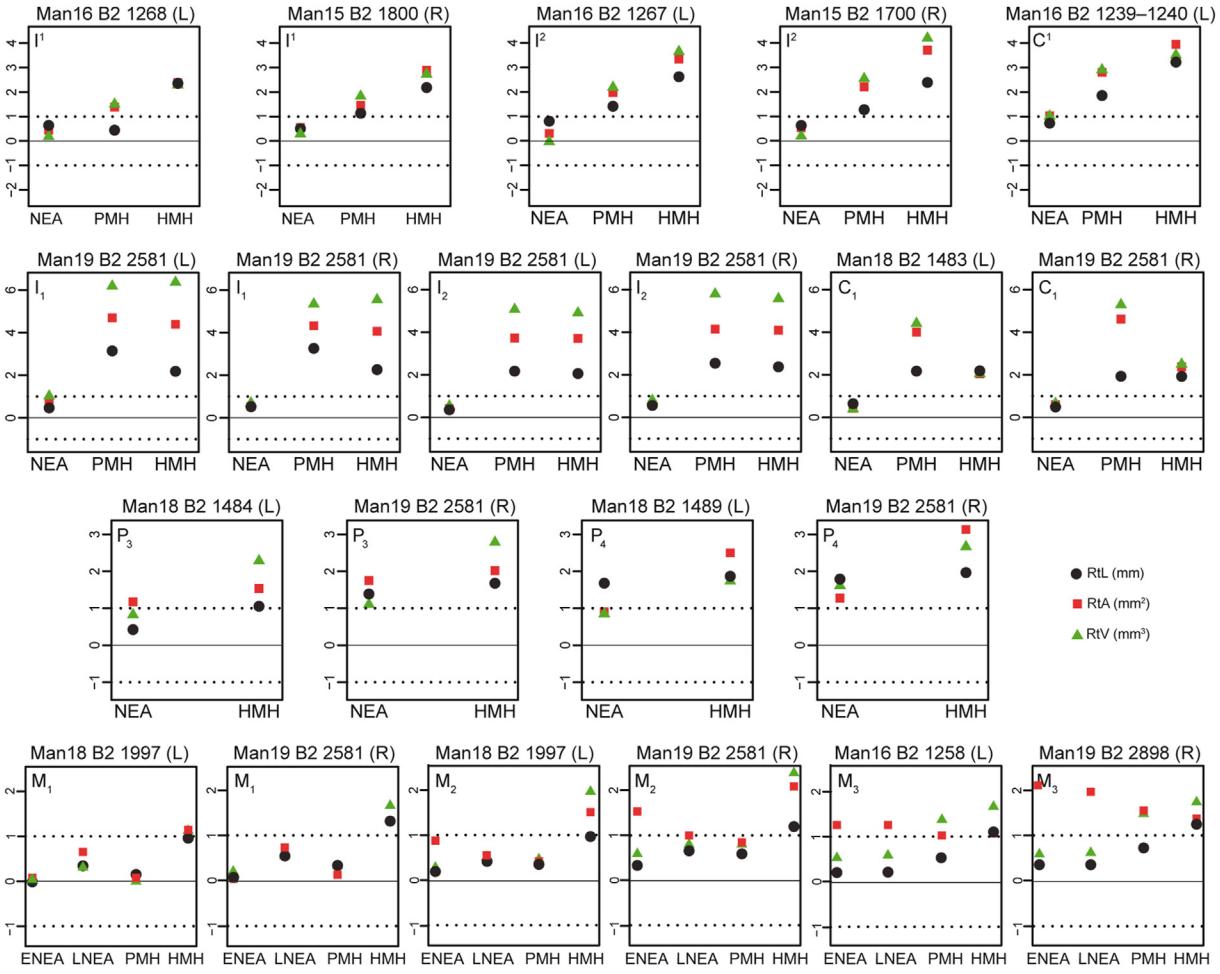

Fig. 12. Adjusted Z-score plots of root length (RtL), root surface area (RtA), and root volume (RtV) of the anterior teeth and mandibular postcanine teeth of Thorin compared to the variation of early Neanderthal (ENEA), late Neanderthal (LNEA), Pleistocene modern humans (PMHs), and Holocene modern humans (HMHs). The solid line passing through 0 represents the mean, and the dotted lines passing through −1.0 and +1.0 represent the 95% limit of the variation of the comparative groups. The accession number of each tooth is indicated above their respective plot (cf. Table 1). Abbreviations: L = left; R = right. (For interpretation of the references to color in this figure, the reader is referred to the Web version of this article.)

Table 4
Volume of root stem (Vstem; in mm^3), volume of root branch (Vbranch; in mm^3), and volume of bifurcation index (VBF; in percentage) of the mandibular molars of Thorin compared with those of early Neanderthals (ENEAs), late Neanderthals (LNEAs), Pleistocene modern human (PMHs), and Holocene modern human (HMHs) samples.[a]

Specimen/group		M_1			M_2			M_3		
		Vstem	Vbranch	VBF	Vstem	Vbranch	VBF	Vstem	Vbranch	VBF
Man18 B2 1997 L		394.75	367.35	51.8	466.8	516.59	47.47			
Man19 B2 2581 R		451.52	438.76	50.72	507.66	628.8	44.67			
Man16 B2 1258 L								526.31	491.94	51.69
Man19 B2 2898 R								415.83	628.27	39.83
ENEA	Mean	457.61	338.37	55.97	667.24	160.96	77.20	712.05	86.56	86.47
	SD	178.77	87.00	11.42	304.83	124.99	18.59	270.46	120.04	18.77
	Range	233.69–826.56	173.34–487.22	46.07–82.66	286.26–1090.70	0.00–301.63	52.85–10.000	372.71–1043.00	0.00–255.12	60.58–100.00
	n	9	9	9	8	8	8	8	8	8
LNEA	Mean	371.54	320.04	53.86	535.51	277.87	67.10	614.04	108.81	83.70
	SD	86.69	81.55	7.35	141.16	163.23	19.98	235.42	98.75	13.86
	Range	250.84–495.95	198.63–399.23	42.24–64.64	353.08–758.62	0.00–416.51	46.18–100.00	417.89–1071.11	0.00–251.43	67.19–100.00
	n	8	8	8	6	6	6	6	6	6
PMH	Mean	357.04	403.31	48.09	463.78	343.28	60.57	403.45	235.50	64.62
	SD	61.75	125.86	6.55	64.45	197.60	18.37	61.65	115.67	15.11
	Range	267.45–390.54	175.73–525.67	10.79–60.94	175.73–525.67	143.03–537.38	46.18–100.00	372.71–1071.11	0.00–255.12	60.58–100.00
	n	11	11	11	9	9	9	8	8	8
HMH	Mean	237.9	274.12	49.27	340.23	124.32	75.75	251.96	128.06	72.84
	SD	58.52	70.09	7.25	146.69	142.36	25.21	50.85	137.93	23.73
	Range	169.33–370.46	153.78–392.48	37.19–66.10	172.97–690.57	0.00–382.47	40.61–100.00	164.62–330.21	0.00–387.11	40.94–100.00
	n	12	12	12	16	16	16	8	8	8

Abbreviations: L = left; R = right; SD = standard deviation.
The accession code is constructed based on the prefix 'Man' for Mandrin, followed by the last two digits of the year of discovery, then by the stratigraphic level in which it was found, and ends with the inventory number.
[a] Comparative data extracted from Kupczik and Hublin (2010) and from Kupczik et al. (2019).

groups (Fig. 14B). Late Neanderthals tend to display more internally placed metaconid and entoconid dentine horns and taller hypoconid and entoconid dentine horns than do the early Neanderthals. The right M_2 of Thorin shows a similar shape as in late Neanderthals and falls close to the M_2 of the mandible from Regourdou. The cross-validated analysis classifies the right M_2 of Thorin as a late Neandertal, with a posterior probability of 100% (Table 5). For M_3s, the CVA plot shows that Neanderthals are separated from Holocene modern humans, but there is some overlap between early and late Neanderthals (Fig. 14C). Early Neanderthals tend to display a more buccolingually compressed EDJ in the occlusal view, with a more internally tilting metaconid dentine horn than in late Neanderthals. As in late Neanderthals, the M_3s of Thorin display a rather broad EDJ shape, especially on the left antimere, falling near the tooth SD 923 from El Sidrón. The cross-validated analysis clearly classifies the M_3s of Thorin with late Neanderthals, with a posterior probability of 98% for the left M_3 and 96% for the right M_3 (Table 5).

4. Discussion

The teeth of Thorin display a series of features that are recognized as typical Neanderthal traits, including shovel-shaped maxillary incisors (Mizoguchi, 1985; Crummett, 1995; Bailey, 2002a, 2002b, 2006; Martinón-Torres et al., 2012), marked labial convexity of the I^1s and I^2s (Bailey, 2006; Bailey and Hublin, 2013; Martinón-Torres et al., 2007, 2012; Scott and Irish, 2017), and a developed tuberculum dentale in the I^1s (Martinón-Torres et al., 2012). It was previously demonstrated that the combination of these three traits in a higher frequency distinguishes the maxillary incisors of Neanderthals from other Pleistocene and Holocene human groups (Bailey and Hublin, 2006). Furthermore, the marginal ridges in the C^1, the well-developed hypocone in the maxillary molars, and the asymmetrical crown of mandibular premolars of Thorin are also more frequently found in Neanderthals than in Pleistocene and Holocene modern humans (Bailey, 2002a, 2002b, 2006; Bailey and Lynch, 2005; Martinón-Torres et al., 2012). The mid-trigonid crest associated with deep anterior fovea in mandibular molars is also more frequently found in Neanderthals than in modern humans (Bailey, 2002a; Bailey et al., 2011; Martinón-Torres et al., 2012; Martínez de Pinillos et al., 2014). The right P_3 of Thorin displays a Tome's root morphology, which is rarely reported for this tooth in Neanderthals (e.g., Valdegoba 1, SJMJ2464; Quam et al., 2001; Compton et al., 2021) and is equally rare in Pleistocene and Holocene humans (Pan and Zanolli, 2019; Compton et al., 2021).

A preliminary description of the nonmetric dental features of some of the teeth of Thorin has been provided in Zanolli (2024). The description of nonmetric dental traits presented in this study is up-to-date and more exhaustive. Indeed, in Zanolli (2024), only the description of the feature at the OES is presented, and the following teeth had not yet been discovered when this previous work was finalized: the left M^1, I_1s, I_2s, right C_1, right P_3 and P_4, and right M_1, M_2, M_3, and M_4. In addition, the present study corrects the lateralization of the upper canine, originally identified as a right antimere, and of the central incisors, initially determined as lateral incisors (and vice versa).

The MD and BL dimensions of Thorin's teeth are systematically closest to those of late Neanderthals than to those of early Neanderthals and Pleistocene and Holocene modern humans. Between MIS 7 and MIS 3, Neanderthals show a dental reduction trend, with the late Neanderthals being characterized by absolutely smaller teeth than early Neanderthals (Voisin et al., 2012). Despite similarities in crown size between late Neanderthal and Pleistocene modern human canines and molars, the BL dimensions of Thorin's incisors and premolars are larger than those of the latter group but close to the average condition of the former.

The results of the geometric morphometric analyses of the EDJ shape indicate that Thorin's molars are morphologically more

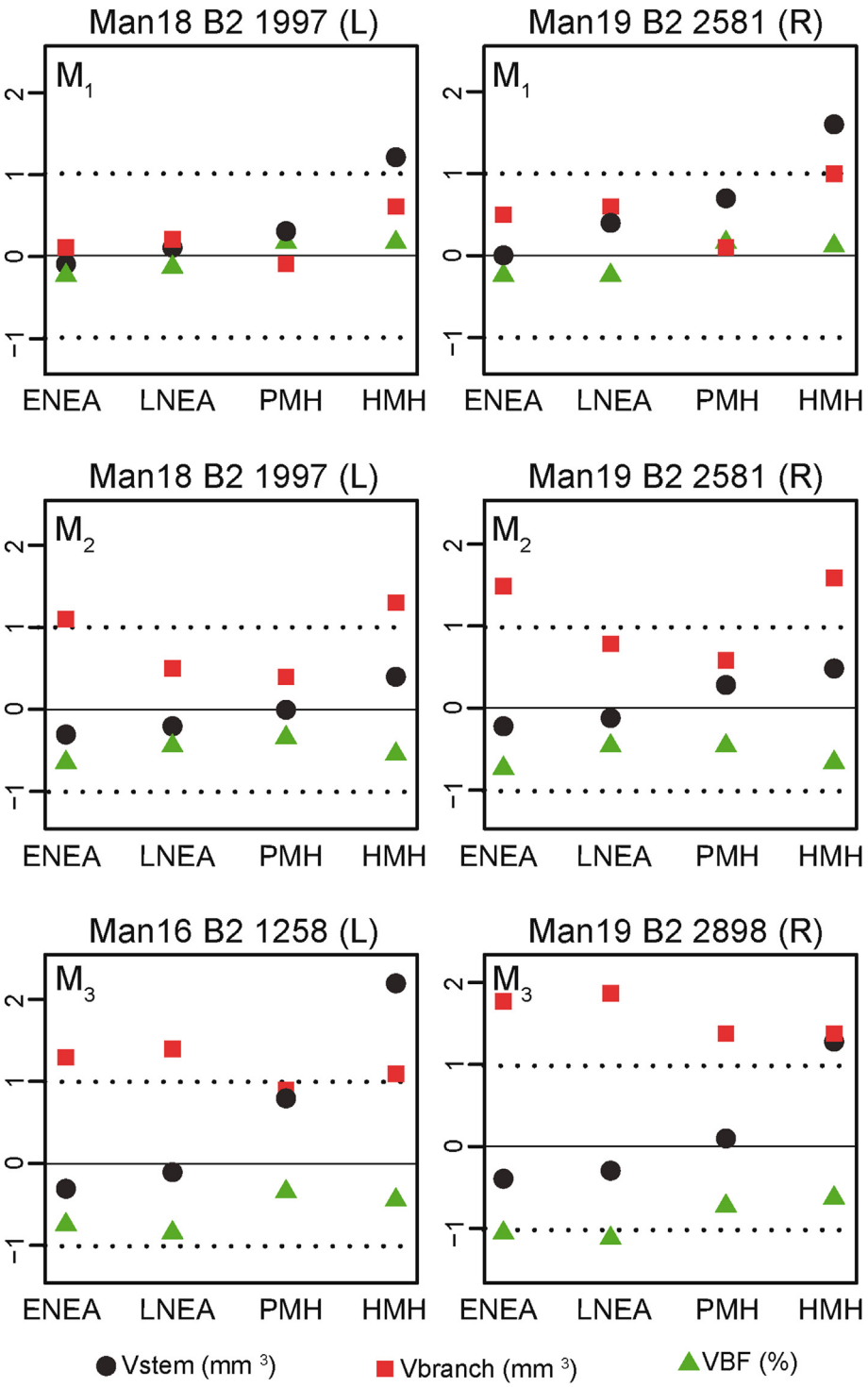

Fig. 13. Adjusted Z-scores plots of root stem (Vstem), volume of root branch (Vbranch), and volume of bifurcation index (VBF) for the mandibular molars of Thorin compared to the variation of early Neanderthal (ENEA), late Neanderthal (LNEA), Pleistocene modern human (PMH), and Holocene modern human (HMH) samples. The solid line passing through 0 represents the mean, and the dotted lines passing through −1.0 and +1.0 represent the 95% limit of the variation of the comparative groups. The accession number of each tooth is indicated above their respective plot (cf. Table 1). Abbreviations: L = left; R = right. (For interpretation of the references to color in this figure, the reader is referred to the Web version of this article.)

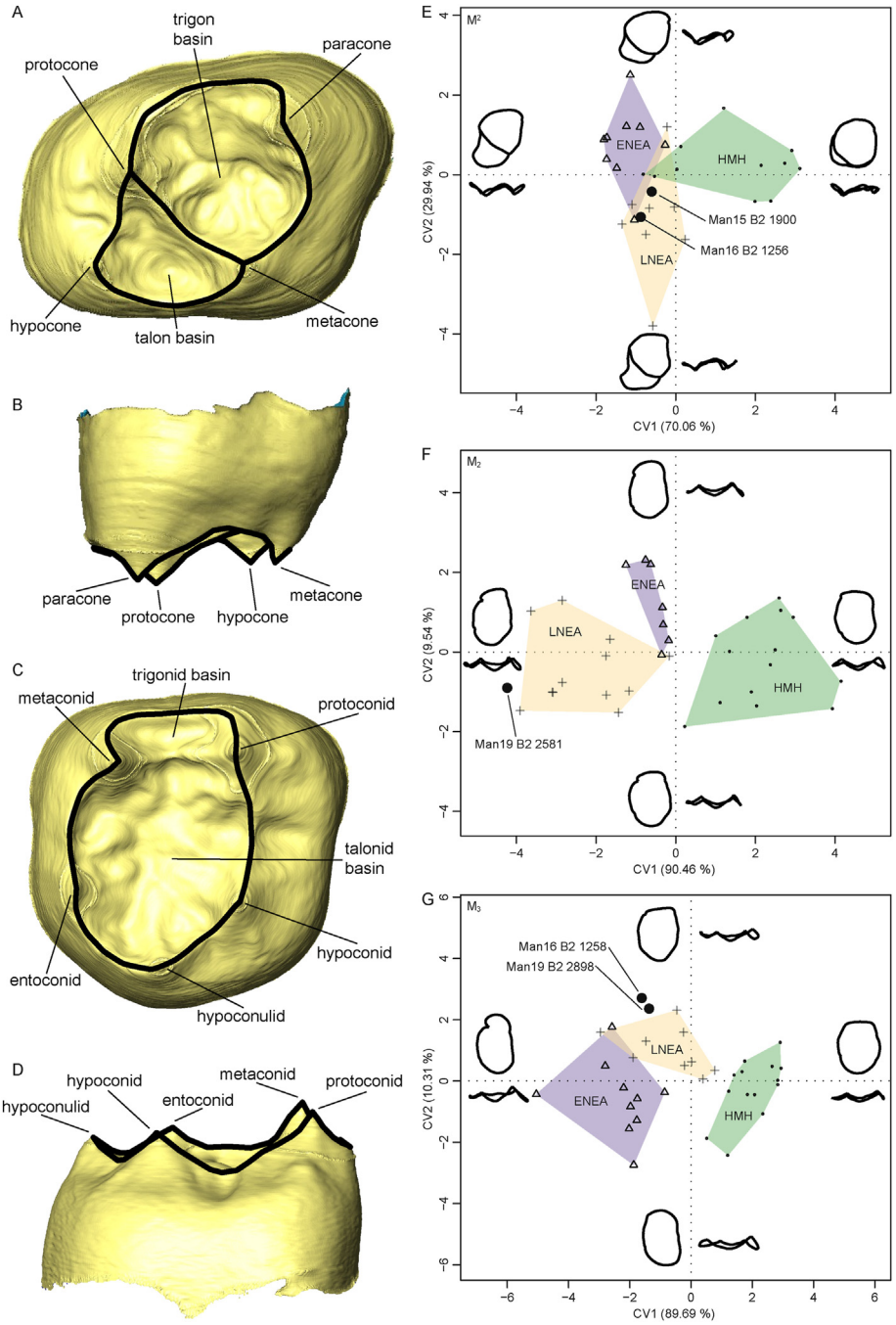

Fig. 14. Illustration of the semilandmark curves positioned on the enamel–dentine junction (EDJ) of Thorin's left M^2 in occlusal (A) and buccal (B) views and of the right M_2 in occlusal (C) and buccal (D) views. Plots of canonical variate 2 (CV2) against canonical variate 1 (CV1) based on the geometric morphometric analysis of the EDJ of Thorin's M^2s (E), right M_2 (F), and M_3s (G) compared to early Neanderthal (ENEA), late Neanderthal (LNEA), and Holocene modern human (HMH) samples. The accession number of each tooth is indicated in the plots (cf. Table 1). (For interpretation of the references to color in this figure, the reader is referred to the Web version of this article.)

similar to those of later Neanderthals than to earlier Neanderthals, even if for M^2s the discrimination between early and late Neanderthals is less clear than for the other molar positions, and Thorin's teeth fall near the range of early Neanderthals. In addition to the analyses of EDJ shape, Thorin's dental dimensions are smaller than in early Neanderthals and are closer to the mean of late Neanderthals. The stem and branch root proportions in the lower molars of Thorin also approximate more the condition of late Neanderthals than that of early Neanderthals.

RtL, RtA, and RtV of anterior teeth are larger for Neanderthals than for Pleistocene and Holocene modern humans (Le Cabec et al., 2013; Augoyard et al., 2023). Similarly, the Neanderthal premolar root size exceeds that of modern humans (Pan et al., 2019), whereas for mandibular molars, early Neanderthals tend to exhibit the largest root size, with late Neanderthals and Late Pleistocene having smaller roots and Holocene humans displaying even more reduced roots (Kupczik and Hublin, 2010; Kupczik et al., 2019). The roots of the anterior teeth of Thorin are rather large and fall within (or even slightly exceed) the known range of variation of early and late Neanderthals. Interestingly, Thorin is characterized by large premolar roots, exceeding the known range for Neanderthals (Table 3; Fig. 12), though this could also be related to the limited

Table 5
Statistics of the cross-validated canonical variate analysis (CVA) based on the geometric morphometric analysis of the enamel–dentine junction (EDJ) shape of the M^2s, right M_2, and M_3s of Thorin.[a]

Group	M^2 EDJ			M_2 EDJ		M_3 EDJ		
	Correct classification	Posterior probability Man16 B2 1256 (L)	Posterior probability Man15 B2 1900 (R)	Correct classification	Posterior probability Man19 B2 2581 (R)	Correct classification	Posterior probability Man16 B2 1258 (L)	Posterior probability Man19 B2 2898 (R)
ENEA	77.8%	15.0%	31.0%	100.0%	0.0%	80.0%	2.0%	3.0%
LNEA	85.5%	82.0%	60.0%	83.3%	100.0%	33.3%	98.0%	97.0%
HMH	63.6%	3.0%	9.0%	78.6%	0.0%	100.0%	0.0%	0.0%

Abbreviations: ENEA = early Neanderthal; LNEA = late Neanderthal; HMH = Holocene modern human; L = left; R = right.
The accession code is constructed based on the prefix 'Man' for Mandrin, followed by the last two digits of the year of discovery, then by the stratigraphic level in which it was found, and ends with the inventory number.
[a] The overall accuracy of correct classification of the EDJs of ENEA, LNEA, and HMH is 75.0% for M^2s, 84.9% for M_2s, and 75.8% for M_3s.

sample size available for comparison (Pan et al., 2019). Similarly, Thorin's left M_1 and M_3 root areas exceed the ranges of early and late Neanderthal, but this could be due to the limited sample size of the comparative samples and, in particular, the lack of Neanderthal representatives from eastern parts of France and Europe. All the teeth of Thorin display also more or less advanced degrees of occlusal wear. In hominins, greater root dimensions (in particular, larger root length and RtA) have been hypothesized to represent a biomechanical adaptation to support occlusal (para)masticatory loads (Schatz et al., 2001; Spencer, 2003; Kupczik and Dean, 2008; Kupczik and Hublin, 2010; Najafzadeh et al., 2024). While the long anterior tooth root of Neanderthals may be an adaptation to better sustain high or frequent loads on the anterior dentition (Le Cabec et al., 2013), this hypothesis has been rejected for postcanine teeth based on finite element analyses, suggesting that the larger and hypertaurodont Neanderthal molar roots are more likely the result of pleiotropy or genetic drift (Clement et al., 2012; Benazzi et al., 2014).

Thorin's dentition, as most Neanderthal teeth, shows thick appositions of cementum or hypercementosis. Hypercementosis is generally defined as an excess of cementum (when the cause is genetic and non-pathological) or abnormal production of cementum (in case of parodontal pathologies), though the etiology of this condition remains unclear (Massé et al., 2023). Several studies have explained the deposition of cementum in past populations as a compensatory response to paramasticatory and nonmasticatory activities such as toothpicking and using the anterior teeth as a 'third hand' (Trinkaus et al., 2008; Martinón-Torres et al., 2011; D'Incau, 2012; Le Cabec et al., 2013; Zanolli et al., 2020; Hernaiz-García et al., 2024). Hypercementosis can also occur on the roots of carious teeth and may be related to periodontal disease (Tillier et al., 1995; D'Incau, 2012; García-González et al., 2019). The dentition of Thorin presents advanced occlusal wear for the anterior teeth, and layers of cementum cover the roots of all teeth, but no dental pathology was observed. The generalized hypercementosis associated with advanced occlusal wear and the presence of bone exostoses on a fragment of maxilla (Zanolli, 2024) suggest an impact of paramasticatory and nonmasticatory activities related to cementum deposition, although a genetic origin cannot be excluded (D'Incau, 2012; Le Cabec et al., 2013; Massé et al., 2023). Indeed, the two distomolars are only moderately worn, and yet an extensive deposit of cementum is present on the apical half of the root, suggesting that intense functional stimuli are not necessary for cementum formation in Neanderthal teeth. Collectively, these observations on Thorin's teeth suggest that perhaps Neanderthals have a genetic predisposition to hypercementosis.

This individual also exhibits a peculiar morphological feature: the presence of two M_4s. To the best of our knowledge, distomolars have never before been described in Neanderthals (or in any other Pleistocene individual of the genus *Homo*; but see Trinkaus, 2018: Supplementary information). The prevalence of supernumerary teeth in contemporary humans ranges from 0.1% to 3.4% according to different studies (Kokten et al., 2003; Ceperuelo et al., 2015; Vázquez Mosquerira et al., 2018). In archeological contexts, supernumerary teeth are rare (especially distomolars): three modern humans with supernumerary premolars from the Postclassic Maya period have been documented in Guatemala (Duncan, 2009); one individual with a supernumerary premolar from the Late Classic Zapotec period was found in Mexico (Duncan, 2009), and one individual with a distomolar was described from levels dated to the Chalcolithic at El Mirador Cave (Ceperuelo et al., 2015). The distomolars of Thorin are heteromorphic, with a single root and a simplified crown. These anomalies occur in the initial stages of dental development. Their etiology is unknown, but several hypotheses have been proposed in the literature (reviewed in Vázquez Mosquerira et al., 2018). Surpernumerary teeth are frequently linked with hyperactivity of dental lamina (Wang and Fan, 2011), syndromes, and diseases (Lubinsky and Kantaputra, 2016), and sex-specific heredity of this character is also another possible factor as some studies documented a higher frequency of appearances in male individuals (Khambete and Kumar, 2012; Ata-Ali et al., 2014). In the absence of any diagnosis of pathology or genetic syndrome, as well as of any information regarding Thorin's closest relatives, these different hypotheses cannot be tested in the present study. In addition, the presence of accessory teeth in primates has been suggested to be a marker of interbreeding (Ackermann, 2010; Ackermann et al., 2014; Harvati and Ackermann, 2022). However, the paleogenetic analysis of Thorin excludes any hybridization with modern humans, a common feature documented for all other late Neanderthals to date (Slimak et al., 2023, 2024c). Developmental disorders, and, in particular, dental anomalies, have also been suggested to result from high levels of consanguinity in Pleistocene populations (Trinkaus, 2018; Ríos et al., 2019).

Considering the paleogenetic data suggesting an early divergence of Thorin's group from other western European Neanderthals and the late chronology of this individual dating to ~44.50–42.25 ka (Slimak et al., 2023, 2024c), Thorin's dental morphology provides crucial information on the paleobiology of one of the last Neanderthals. At least one incursion of modern humans is documented in Western Europe around 54 ka at Grotte Mandrin (Slimak et al., 2022), and multiple other modern human groups dispersed from Africa and western Asia to Europe from 48 ka onwards (Hublin et al., 2020). There are only a limited number of Neanderthal remains dating to the few millennia before their disappearance and for this reason; Thorin is thus key to better understanding the paleobiology of the latest Neanderthals. The analysis of Thorin's DNA highlighted a deep divergence of his group from other Neanderthal groups, showing genetic affinities with eastern Neanderthals dating to 100–80 ka (Slimak et al., 2023).

Another Neanderthal individual from Gibraltar Forbe's Quarry also presents a deep divergence from other late European Neanderthals (Bokelmann et al., 2019) and possibly belongs to the same deme as Thorin and his relatives (Slimak et al., 2023). However, the specimen Gibraltar 1 only preserves the anterior dentition, which is heavily worn, thus preventing any morphological comparison with Thorin's teeth. The study of Thorin's DNA revealed that he belonged to an isolated group of Neanderthals, which would thus support the latter hypothesis. However, more (paleo)genetic analyses of hominins, as well as a better understanding of genotype–phenotype relationships, are needed to test this further.

5. Conclusions

The dentition of the adult individual Thorin from Grotte Mandrin, dated to approximately ~52–42 ka, displays dental structural features typical of those of Neanderthals from MIS 5–3, even if it shows large premolar roots compared with the known range of Neanderthals. The teeth of Thorin display advanced occlusal wear, especially for the anterior teeth, which suggests the involvement of his teeth in paramasticatory or nonmasticatory activities, but this remains to be tested by investigating microwear patterns on the labial surface of the enamel (Volpato et al., 2012). The presence of distomolars, combined with the early genetic divergence computed for Thorin (Slimak et al., 2023, 2024c), make this adult male Neanderthal an intriguing individual. Further research on his paleobiology, and the paleoenvironment and cultural aspects of his group, will likely shed light on the life of the last Neanderthals of the Rhône Valley.

CRediT authorship contribution statement

Jeanne Fuchs: Writing – original draft, Visualization, Validation, Methodology, Funding acquisition, Formal analysis. **Antonio García-Tabernero:** Data curation. **Antonio Rosas:** Writing – review & editing, Data curation. **Hubert Camus:** Writing – review & editing. **Laure Metz:** Writing – review & editing. **Ludovic Slimak:** Writing – original draft, Visualization, Validation, Supervision, Resources, Project administration, Investigation, Funding acquisition, Conceptualization. **Clément Zanolli:** Writing – original draft, Validation, Supervision, Resources, Methodology, Funding acquisition, Data curation, Conceptualization.

Acknowledgments

We deeply thank the Service Régional de l'Archéologie Auvergne Rhône-Alpes and the city of Malataverne that supported the 34 years of continuous field research in Grotte Mandrin. We also thank the many curators and colleagues who granted access to the comparative fossil and recent hominin specimens for scanning, as well as the online sharing platforms of the Nespos Society and ESRF Paleontological database (http://paleo.esrf.eu). For analytical support and microtomographic scanning and sharing of the material, we acknowledge B. Duployer and C. Tenailleau (University of Toulouse); A. Mazurier and R. Macchiarelli (University of Poitiers); M. Honegger (University of Neuchâtel); F. Bon and J. Cauliez (University of Toulouse J. Jaurès); S. Hérouin (Archeological Service of Chartres); R. Lebrun (University of Montpellier); A. Bravin, C. Nemoz, and P. Tafforeau (ESRF Synchrotron); P. Bayle, I. Crevecoeur, A. Le Cabec, R. Ledevin, B. Maureille, S. Rottier, and F. Santos (University of Bordeaux), P. Sémal (Royal Belgian Institute of Natural Sciences). This study received financial support from the French government in the framework of the University of Bordeaux's IdEx "Investments for the Future" program/GPR "Human Past." It was also funded by the city of Malataverne (Drôme, France) and the department of Drôme. The Spanish Ministry of Science and Innovation funds partial aspects of this research via PID 2021-122356NB-I00. Finally, we acknowledge the Editor-in-Chief (Andrea Taylor), Associate Editor, and three anonymous reviewers for helpful comments and suggestions that helped us improve this paper.

Supplementary Online Material

Supplementary Online Material to this article can be found online at https://doi.org/10.1016/j.jhevol.2024.103599.

References

Ackermann, R.R., 2010. Phenotypic traits of primate hybrids: Recognizing admixture in the fossil record. Evol. Anthropol. 19, 258–270.

Ackermann, R.R., Schroeder, L., Rogers, J., Cheverud, J.M., 2014. Further evidence for phenotypic signatures of hybridization in descendant baboon populations. J. Hum. Evol. 76, 54–62.

Allentoft, M.E., Sikora, M., Refoyo-Martínez, A., Irving-Pease, E.K., Fischer, A., Barrie, W., Ingason, A., Stenderup, J., Sjögren, K.-G., Pearson, A., Mota, B., Paulsson, B.S., Halgren, A., Macleod, R., Schjellerup Jørkov, M.L., Demeter, F., Novosolov, M., Sørensen, L., Nielsen, P.-O., Henriksen, R.H.A., Vimala, T., McColl, H., Margaryan, A., Ilardo, M., Vaughn, A., Mortensen, M.F., Nielsen, A.B., Hede, M.U., Rasmussen, P., Vinner, L., Renaud, G., Stern, A., Trolle Jensen, T.Z., Johannsen, N.N., Scorrano, G., Schroeder, H., Lysdahl, P., Ramsøe, A.D., Skorobogatov, A., Schork, A.J., Rosengren, A., Ruter, A., Outram, A., Timoshenko, A.A., Buzhilova, A., Coppa, A., Zubova, A., Silva, A.M., Hansen, A.J., Gromov, A., Logvin, A., Gotfredsen, A.B., Nielsen, B.H., González-Rabanal, B., Lalueza-Fox, C., McKenzie, C.J., Gaunitz, C., Blasco, C., Liesau, C., Martinez-Labarga, C., Pozdnyakov, D.V., Cuenca-Solana, D., Lordkipanidze, D.O., En'shin, D., Salazar-García, D.C., Price, T.D., Borić, D., Kostyleva, E., Veselovskaya, E.V., Usmanova, E.R., Cappellini, E., Petersen, E.B., Kannegaard, E., Radina, F., Yediay, F.E., Duday, H., Gutiérrez-Zugasti, I., Potekhina, I., Shevnina, I., Altinkaya, I., Guilaine, J., Hansen, J., Tortosa, J.E.A., Zilhão, J., Vega, J., Pedersen, K.B., Tunia, K., Zhao, L., Mylnikova, L.N., Larsson, L., Metz, L., Yeppiskoposyan, L., Pedersen, L., Sarti, L., Orlando, L., Slimak, L., Klassen, L., Blank, M., González-Morales, M., Silvestrini, M., Vretemark, M., Nesterova, M.S., Rykun, M., Rolfo, M.F., Szmyt, M., Przybyła, M., Calattini, M., Sablin, M., Dobisíková, M., Meldgaard, M., Johansen, M., Berezina, N., Card, N., Saveliev, N.A., Poshekhonova, O., Rickards, O., Lozovskaya, O.V., Uldum, O.C., Aurino, P., Kosintsev, P., Courtaud, P., Ríos, P., Mortensen, P., Lotz, P., Persson, P.Å., Bangsgaard, P., Damgaard, P.D.B., Petersen, P.V., Martinez, P.P., Włodarczak, P., Smolyaninov, R.V., Maring, R., Menduiña, R., Badalyan, R., Iversen, R., Turin, R., Vasilyiev, S., Wåhlin, S., Borutskaya, S., Skochina, S., Sørensen, S.A., Andersen, S.H., Jørgensen, T., Serikov, Y.B., Molodin, V.I., Smrcka, V., Merz, V., Appadurai, V., Moiseyev, V., Magnusson, Y., Kjær, K.H., Lynnerup, N., Lawson, D.J., Sudmant, P.H., Rasmussen, S., Korneliussen, T., Durbin, R., Nielsen, R., Delaneau, O., Werge, T., Racimo, F., Kristiansen, K., Willerslev, E., 2022. Population genomics of Stone age Eurasia. bioRxiv preprint. available at: https://doi.org/10.1101/2022.05.04.490594.

Ata-Ali, F., Ata-Ali, J., Peñarrocha-Oltra, D., Peñarrocha-Diago, M., 2014. Prevalence, etiology, diagnosis, treatment and complications of supernumerary teeth. J. Clin. Exp. Dent. 6, e414–e418.

Augoyard, M., Zanolli, C., Santos, F., Oettlé, A.C., L'Abbé, E.N., Le Luyer, M., Cazenave, M., Colard, T., Hoffman, J., Profico, A., Bayle, P., 2023. Evaluation of age, sex, and ancestry-related variation in cortical bone and dentine volumes in modern humans, and a preliminary assessment of cortical bone-dentine covariation in later *Homo*. J. Anthropol. Sci. 100, 143–169.

Bailey, S.E., 2002a. Neandertal dental morphology: Implications for modern human origins. Ph.. D. Dissertation, Arizona State University.

Bailey, S.E., 2002b. A closer look at Neandertal postcanine dental morphology: the mandibular dentition. Anat. Rec. 269, 148–156.

Bailey, S.E., 2006. The evolution of non-metric dental variation in Europe. Mitt. Ges. Urgesch. 15, 9–30.

Bailey, S.E., Lynch, J.M., 2005. Diagnostic differences in mandibular P4 shape between Neandertals and anatomically modern humans. Am. J. Phys. Anthropol. 126, 268–277.

Bailey, S.E., Hublin, J.-J., 2006. Dental remains from the Grotte du Renne at Arcy-sur-Cure (Yonne). J. Hum. Evol. 50, 485–508.

Bailey, S.E., Hublin, J.-J., 2013. What does it mean to be dentally 'modern'? In: Scott, G.R., Irish, J.D. (Eds.), Anthropological Perspectives on Tooth Morphology, Genetics, Evolution, Variation. Cambridge University Press, Cambridge, pp. 222–249.

Bailey, S.E., Skinner, M.M., Hublin, J.-J., 2011. What lies beneath? An evaluation of lower molar trigonid crest patterns based on both dentine and enamel expression. Am. J. Phys. Anthropol. 145, 505–518.

Benazzi, S., Douka, K., Fornai, C., Bauer, C.C., Kullmer, O., Svoboda, J., Pap, I., Mallegni, F., Bayle, P., Coquerelle, M., Condemi, S., Ronchitelli, A., Harvati, K.,

Weber, G.W., 2011. Early dispersal of modern humans in Europe and implications for Neanderthal behaviour. Nature 479, 525–528.
Benazzi, S., Nguyen, H.N., Kullmer, O., Hublin, J.-J., 2014. Exploring the biomechanics of taurodontism. J. Anat. 226, 180–188.
Benazzi, S., Slon, V., Talamo, S., Negrino, F., Peresani, M., Bailey, S.E., Sawyer, S., Panetta, D., Vicino, G., Starnini, E., Mannino, M.A., Salvadori, P.A., Meyer, M., Paabo, S., Hublin, J.-J., 2015. The makers of the Protoaurignacian and implications for Neandertal extinction. Science 348, 793–796.
Bokelmann, L., Hajdinjak, M., Peyrégne, S., Brace, S., Essel, E., de Filippo, C., Glocke, I., Grote, S., Mafessoni, F., Nagel, S., Kelso, J., Prüfer, K., Vernot, B., Barnes, I., Pääbo, S., Meyer, M., Stringer, C., 2019. A genetic analysis of the Gibraltar Neanderthals. Proc. Natl. Acad. Sci. USA 116, 15610–15615.
Cardini, A., Polly, P.D., 2020. Cross-validated between group PCA scatterplots: a solution to spurious group separation? Evol. Biol. 47, 85–95.
Caron, F., d'Errico, F., Del Moral, P., Santos, F., Zilhão, J., 2011. The reality of Neandertal symbolic behavior at the Grotte du Renne, Arcy-sur-Cure, France. PLoS One 6, e21545.
Ceperuelo, D., Lozano, M., Duran-Sindreu, F., Mercadé, M., 2015. Supernumerary fourth molar and dental pathologies in a Chalcolithic individual from the El Mirador Cave site (Sierra de Atapuerca, Burgos, Spain). J. Comp. Hum. Evol. 66, 15–26.
Clement, A.F., Hillson, S.W., Aiello, L.C., 2012. Tooth wear, Neanderthal facial morphology and the anterior dental loading hypothesis. J. Hum. Evol. 62, 367–376.
Compton, T., Skinner, M.M., Humphrey, L., Pope, M., Bates, M., Davies, T.W., Parfitt, S.A., Plummer, W.P., Scott, B., Shaw, A., Stringer, C., 2021. The morphology of the Late Pleistocene hominin remains from the site of La Cotte de St Brelade, Jersey (Channel Islands). J. Hum. Evol. 152, 102939.
Coqueugniot, H., Dutour, O., 2024, In press. Etude des éléments du squelette de la main de Thorin. In: Slimak, L., Giraud, Y., Metz, L., Yvorra, P. (Eds.), Mandrin, des Derniers Néandertaliens aux Premiers Humains Modernes en France Méditerranéenne. Artisanats et Territoires, Aix-en-Provence, pp. 676–681.
Crummett, T., 1995. The three dimensions of shovel-shaping. In: Moggi-Cecchi, J. (Ed.), Aspects of Dental Biology: Palaeontology, Anthropology and Evolution.International. Institute for the Study of Man, Florence, pp. 305–313.
Davies, T.W., Alemseged, Z., Gidna, A., Hublin, J.-J., Kimbel, W.H., Kullmer, O., Spoor, F., Zanolli, C., Skinner, M.M., 2021. Accessory cusp expression at the enamel-dentine junction of hominin mandibular molars. PeerJ 9, e11415.
d'Errico, F., Zilhão, J., Julien, M., Baffier, D., Pelegrin, J., 1998. Neanderthal acculturation in western Europe? A critical review of the evidence and its interpretation. Curr. Anthropol. 39, S1–S44.
Devièse, T., Abrams, G., Hadjinjak, M., Pirson, S., De Groote, I., Di Modica, K., Toussaint, M., Fisher, V., Comeskey, D., Spindler, L., Meyer, M., Semal, P., Higham, T., 2021. Reevaluating the timing of Neanderthal disappearance in Northwest Europe. Proc. Natl. Acad. Sci. USA 118, e2022466118.
D'Incau, E., 2012. Hypercémentose: Définition, classification et fréquence apport des résultats à la lignée néandertalienne. Ph.D. Dissertation, Université Bordeaux 1.
Duncan, W.N., 2009. Supernumerary teeth from two Mesoamerican archaeological contexts. Dent. Anthropol. 22, 39–46.
García-González, R., Sanchez-Puente, Z., Rodríguez, L., Quam, R.M., Carretero, J.M., 2019. Hypercementosis of the Magdalenian human mandibular teeth from El Mirón cave, Cantabria (Spain). Quat. Sci. Rev. 515, 150–158.
Gicqueau, A., Schuh, A., Henrion, J., Viola, B., Partiot, C., Guillon, M., Golovanova, L., Doronichev, V., Gunz, P., Hublin, J.-J., Maureille, B., 2023. Anatomically modern human in the Châtelperronian hominin collection from the Grotte du Renne (Arcy-sur-Cure, Northeast France). Sci. Rep. 13, 12682.
Giraud, Y., Brugal, J.P., Jeannet, M., 1998. Un nouveau gisement moustérien en moyenne vallée du Rhône: La grotte Mandrin à Malataverne (Drôme). Bull. Soc. Prehist. Fr. 95, 7–16.
Gravina, B., Bachellerie, F., Caux, S., Discamps, E., Faivre, J.-P., Galland, A., Michek, A., Teyssandier, N., Bordes, J.-G., 2018. No reliable evidence for a Neanderthal-Châtelperronian association at La Roche-à-Pierrot, Saint-Césaire. Sci. Rep. 8, 15134.
Harvati, K., Ackermann, R.R., 2022. Merging morphological and genetic evidence to assess hybridization in Western Eurasian late Pleistocene hominins. Nat. Ecol. Evol. 6, 1573–1585.
Hernaiz-García, M., Zanolli, C., Martín-Francés, L., Mazurier, A., Benazzi, S., Sarig, R., Fu, J., Kullmer, O., Fiorenza, L., 2024. Masticatory habits of the adult Neanderthal individual BD 1 from La Chaise-de-Vouthon (France). Am. J. Biol. Anthropol. 184, e24926.
Higham, T., Douka, K., Wood, R., Ramsey, C.B., Brock, F., Basell, L., Camps, M., Arrizabalaga, A., Baena, J., Barroso-Ruíz, C., Bergman, C., Boitard, C., Boscato, P., Caparrós, M., Conard, N.J., Draily, C., Froment, A., Galván, B., Gambassini, P., Garcia-Moreno, A., Grimaldi, S., Haesaerts, P., Holt, B., Iriarte-Chiapusso, M.-J., Jelinek, A., Jordá Pardo, J.F., Maíllo-Fernández, J.-M., Marom, A., Maroto, J., Menéndez, M., Metz, L., Morin, E., Moroni, A., Negrino, F., Panagopoulou, E., Peresani, M., Pirson, S., de la Rasilla, M., Riel-Salvatore, J., Ronchitelli, A., Santamaria, D., Semal, P., Slimak, L., Soler, J., Soler, N., Villaluenga, A., Pinhasi, R., Jacobi, R., 2014. The timing and spatiotemporal patterning of Neanderthal disappearance. Nature 512, 306–309.
Hublin, J.-J., Sirakov, N., Aldeias, Bailey, S., Bard, E., Delvignes, V., Endarova, E., Fagault, Y., Fewlass, H., Hajdinjak, M., Kromer, B., Krumov, I., Marreiros, J., Martisius, N.L., Paskulin, L., Sinet-Mathiot, V., Meyer, M., Pääbo, S., Popov, V., Rezek, Z., Sirakova, S., Skinner, M.M., Smith, G.M., Spasov, R., Talamo, S., Tuna, T., Wacker, F., Wilcke, A., Zahariev, N., McPherron, S.P., Tsanova, T., 2020. Initial Upper Palaeolithic *Homo sapiens* from Bacho Kiro Cave, Bulgaria. Nature 581, 299–302.
Hublin, J.-J., 2015. The modern human colonization of western Eurasia: When and where? Quat. Sci. Rev. 118, 194–210.
Hublin, J.-J., Mylopotamitaki, D., Fewlass, H., Zavala, E.I., Rougier, H., Sümer, A.p., Hajdinjak, M., Smith, G.M., Ruebens, K., Sinet-Mathiot, V., Pederzani, S., Harking, F., Olsen, J.V., Kirchner, A., Lauer, T., Stahlschmidt, M., Hein, M., Talamo, S., Meller, H., Diet, H., Orschied, J., Prüfer, K., Krause, J., Meyer, M., Welker, F., McPherron, S.P., Schüler, T., Weiss, M., 2023. Who were the makers of the Lincombian-Ranisian-Jerzmanowician? New evidence from the site of Ilsenhöhle in Ranis (Germany). PaleoAnthropology 2023, 332.
Irish, J.D., Guatelli-Steinberg, D., Legge, S.S., De Ruiter, D.J., Berger, L.R., 2013. Dental morphology and the phylogenetic "place" of *Australopithecus sediba*. Science 340, 1233062.
Khambete, N., Kumar, R., 2012. Genetics and presence of non-syndromic supernumerary teeth: a mystery case report and review of literature. Contemp. Clin. Dent. 3, 499–502.
Kokten, G., Balcioglu, H., Buyukertan, M., 2003. Supernumerary fourth and fifth molars: a report of two cases. J. Contemp. Dent. Pract. 4, 2–5.
Kupczik, K., Dean, M.C., 2008. Comparative observations on the tooth root morphology of *Gigantopithecus blacki*. J. Hum. Evol. 54, 196–204.
Kupczik, K., Hublin, J.-J., 2010. Mandibular molar root morphology in Neanderthals and Late Pleistocene and recent *Homo sapiens*. J. Hum. Evol. 59, 525–541.
Kupczik, K., Delezene, L.K., Skinner, M.M., 2019. Mandibular molar root and pulp cavity morphology in *Homo naledi* and other Plio-Pleistocene hominins. J. Hum. Evol. 130, 83–95.
Leroi-Gourhan, A., 1965. Le Châtelperronien, problème ethnologique. In: Ripoll Perelló, E. (Ed.), Miscelanea en Homenaje al Abate Henri Breuil (1877-1961). Instituto de prehistoria y arqueologia, Barcelona, pp. 75–81.
Le Cabec, A., Gunz, P., Kupczik, K., Braga, J., Hublin, J.-J., 2013. Anterior tooth root morphology and size in Neanderthals: Taxonomic and functional implications. J. Hum. Evol. 64, 169–193.
Lubinsky, M., Kantaputra, P.-N., 2016. Syndromes with supernumerary teeth. Am. J. Med. Genet. A 170, 2611–2616.
Martin, R.M.G., Hublin, J.-J., Gunz, P., Skinner, M.M., 2017. The morphology of the enamel–dentine junction in Neanderthal molars: Gross morphology, nonmetric traits, and temporal trends. J. Hum. Evol. 103, 20–44.
Martínez de Pinillos, M., Martinón-Torres, M., Skinner, M.M., Arsuaga, J.L., Gracia-Téllez, A., Martínez, I., Martín-Francés, L., Bermúdez de Castro, J.M., 2014. Trigonid crests expression in Atapuerca-Sima de los Huesos lower molars: Internal and external morphological expression and evolutionary inferences. C. R. Palevol. 13, 205–221.
Martinón-Torres, M., Bermúdez de Castro, J., Gómez-Robles, A., Sarmiento, S., Muela, A., Arusaga, J.L., 2007. Gran Dolina-TD6 and Sima de los Huesos dental samples: Preliminary approach to some dental characters of interest for phylogenetic studies. In: Bailey, S.E., Hublin, J.-J. (Eds.), Dental Perspectives on Human Evolution. Springer-Verlag, Berlin, pp. 65–79.
Martinón-Torres, M., Martínez de Pinillos, M., Skinner, M.M., Martín-Francés, L., Gracia-Téllez, A., Martínez, I., Arsuaga, J.L., Bermúdez de Castro, J.M., 2014. Talonid crests expression at the enamel-dentine junction of hominin lower permanent and deciduous molars. C.R. Palevol. 13, 223–234.
Martinón-Torres, M., Martín-Francés, L., Gracia, A., Olejniczak, A., Prado-Simón, L., Gómez-Robles, A., Lapresa, M., Carbonell, E., Arsuaga, J.L., Bermúdez De Castro, J.M., 2011. Early Pleistocene human mandible from Sima del Elefante (TE) cave site in Sierra de Atapuerca (Spain): A palaeopathological study. J. Hum. Evol. 61, 1–11.
Martinón-Torres, M., Bermúdez De Castro, J.M., Gómez-Robles, A., Prado-Simón, L., Arsuaga, J.L., 2012. Morphological description and comparison of the dental remains from Atapuerca-Sima de los Huesos site (Spain). J. Hum. Evol. 62, 7–58.
Massé, L., Garot, E., Maureille, B., Le Cabec, A., 2023. Insights into the aetologies of hypercementosis: a systematic review and a scoring system. Arch. Oral Biol. 146, 105599.
Maureille, B., Rougier, H., Houët, F., Vandermeersch, B., 2001. Les dents inférieures du néandertalien Regourdou 1 (site de Regourdou, commune de Montignac, Dordogne): Analyses métriques et comparatives. PALEO 13, 183–200.
Mellars, P., 2004. Neanderthals and the modern human colonization of Europe. Nature 432, 461–465.
Metz, L., Lewis, J.E., Slimak, L., 2023. Bow-and-arrow, technology of the first modern humans in Europe 54,000 years ago at Mandrin, France. Sci. Adv. 9, eadd4675.
Mizoguchi, Y., 1985. Shoveling: A Statistical Analysis of its Morphology. University of Tokyo Press, Tokyo.
Moroni, A., Ronchitelli, A., Arrighi, S., Aureli, D., Bailey, S., Boscato, P., Boschin, F., Capecchi, G., Crezzini, J., Douka, K., Marciani, G., Panetta, D., Ranaldo, F., Ricci, S., Scaramucci, S., Spagnolo, V., Benazzi, S., Gambassini, P., 2018. Grotta del Cavallo (Apulia-Southern Italy). The Uluzzian in the mirror. J. Anthropol. Sci. 96, 125–160.
Najafzadeh, A., Hernaiz-García, M., Benazzi, S., Chen, B., Hublin, J.-J., Kullmer, O., Pokhojaev, A., Sarig, R., Sorrentino, R., Vazzana, A., Fiorenza, L., 2024. Finite element analysis of Neanderthal and early *Homo sapiens* maxillary central incisor. J. Hum. Evol. 189, 103512.
Olejniczak, A.J., Tafforeau, P., Feeney, R.N.M., Martin, L.B., 2008. Three-dimensional primate molar enamel thickness. J. Hum. Evol. 54, 187–195.
Ortiz, A., Skinner, M.M., Bailey, S.E., Hublin, J.-J., 2012. Carabelli's trait revisited: an examination of mesiolingual features at the enamel–dentine junction and

enamel surface of *Pan* and *Homo sapiens* upper molars. J. Hum. Evol. 63, 586–596.
Ortiz, A., Bailey, S.E., Schwartz, G.T., Hublin, J.-J., Skinner, M.M., 2018. Evo-devo models of tooth development and the origin of hominoid molar diversity. Sci. Adv. 4, eaar2334.
Oxilia, G., Bortolini, E., Marciani, G., Menghi Sartorio, J.C., Bettuzzi, M., Panetta, D., Arrighi, S., Badino, F., Figus, C., Lugli, F., Romandini, M., Silvestrini, S., Sorrentino, R., Moroni, A., Donadio, C., Morigi, M.P., Slon, V., Piperno, M., Talamo, S., Collina, C., Benazzi, S., 2022. Direct evidence that late Neanderthal occupation precedes a technological shift in southwestern Italy. Am. J. Biol. Anthropol. 179, 18–30.
Palma di Cesnola, A., 1989. L'Uluzzien: Faciès italien du Leptolithique archaïque. L'Anthropologie 93, 783–812.
Pan, L., Zanolli, C., 2019. Comparative observations on the premolar root and pulp canal configurations of Middle Pleistocene *Homo* in China. Am. J. Phys. Anthropol. 168, 637–646.
Pan, L., Dumoncel, J., Mazurier, A., Zanolli, C., 2019. Structural analysis of premolar roots in Middle Pleistocene hominins from China. J. Hum. Evol. 136, 102669.
Pelegrin, J., 1995. Technologie Lithique: Le Châtelperronien de Roc de Combe (Lot) et de La Côte (Dordogne). CNRS editions, Paris.
Quam, R.M., Arsuaga, J.-L., Bermúdez de Castro, J.M., Díez, J.C., Lorenzo, C., Carretero, J.M., García, N., Ortega, A.I., 2001. Human remains from Valdegoba Cave (Huérmeces, Burgos, Spain). J. Hum. Evol. 41, 385–435.
R Core Team, 2023. R: A Language and Environment for Statistical Computing. R Foundation for Statistical Computing, Vienna.
Ríos, L., Kivell, T.L., Lalueza-Fox, C., Estalrrich, A., García-Tabernero, A., Huguet, R., Quintino, Y., de la Rasilla, M., Rosas, A., 2019. Skeletal anomalies in the Neandertal family of El Sidrón (Spain) support a role of inbreeding in Neandertal extinction. Sci. Rep. 9, 1697.
Ruebens, K., McPherron, S.J.P., Hublin, J.-J., 2015. On the local Mousterian origin of the Châtelperronian: Integrating typo-technological, chronostratigraphic and contextual data. J. Hum. Evol. 86, 55–91.
Schatz, D., Alfter, G., Göz, G., 2001. Fracture resistance of human incisors and premolars: morphological and patho-anatomical factors. Dent. Traumatol. 17, 167–173.
Semal, P., Rougier, H., Crevecoeur, I., Jungels, C., Flas, D., Hauzeur, A., Maureille, B., Germonpré, M., Bocherens, H., Pirson, S., Cammaert, L., De Clerck, N., Hambucken, A., Higham, T., Toussaint, M., van der Plicht, J., 2009. New data on the late Neandertals: direct dating of the Belgian Spy fossils. Am. J. Phys. Anthropol. 138, 421–428.
Schlager, S., 2023. Morpho: calculations and visualizations related to geometric morphometrics. R package version 2.11. http://cran.r-project.org/web/packages/Morpho/index.html.
Scolan, H., Santos, F., Tillier, A.-M., Maureille, B., Quintard, A., 2012. Des nouveaux vestiges néeanderthaliens à Las Pélénos (Monsempron-Libos, Lot-et-Garonne, France). Bull. Mem. Soc. Anthropol. Paris 24, 69–95.
Scott, G.R., Irish, J.D., 2017. Human Tooth Crown and Root Morphology: the Arizona State University Dental Anthropology System, first ed. Cambridge University Press, Cambridge.
Skinner, M.M., Wood, B.A., Boesch, C., Olejniczak, A.J., Rosas, A., Smith, T.M., Hublin, J.-J., 2008. Dental trait expression at the enamel-dentine junction of lower molars in extant and fossil hominoids. J. Hum. Evol. 54, 173–186.
Slimak, L., 2004. Les dernières expressions du Moustérien entre Loire et Rhône. Ph.D. Dissertation, Université de Provence.
Slimak, L., 2008. Le Néronien et la structure historique du basculement du Paléolithique moyen au Paléolithique supérieure en France méditerranéenne. C. R. Palevol. 6, 301–309.
Slimak, L., 2019. For a cultural anthropology of the last Neanderthals. Quat. Sci. Rev. 217, 330–339.
Slimak, L., 2023. The three waves: Rethinking the structure of the first upper Paleolithic in western Eurasia. PLoS One 18, e0277444.
Slimak, L., Pesesse, D., Giraud, Y., 2006. Reconnaissance d'une installation du Protoaurignacien en vallée du Rhône. Implications sur nos connaissances concernant les premiers hommes modernes en France méditerranéenne. C. R. Palevol. 5, 909–917.
Slimak, L., Zanolli, C., Higham, T., Frouin, M., Schwenninger, J.-L., Arnold, L.J., Demuro, M., Douka, K., Mercier, N., Guérin, G., Valladas, H., Yvorra, P., Giraud, Y., Seguin-Orlando, A., Orlando, L., Lewis, J.E., Muth, X., Camus, H., Vandevelde, S., Buckley, M., Mallol, C., Stringer, C., Metz, L., 2022. Modern human incursion into Neanderthal territories 54,000 years ago at Mandrin, France. Sci. Adv. 8, eabj9496.
Slimak, L., Vimala, T., Seguin-Orlando, A., Metz, L., Zanolli, C., Joannes-Boyau, R., Frouin, M., Arnold, L.J., Demuro, M., Devièse, T., Comeskey, D., Buckley, M., Camus, H., Muth, X., Lewis, J.E., Bocherens, H., Yvorra, P., Tenailleau, C., Duployer, B., Coqueugniot, H., Dutour, O., Higham, T., Sikora, M., 2023. A late Neanderthal reveals genetic isolation in their populations before extinction. bioRxiv preprint. https://doi.org/10.1101/2023.04.10.536015.
Slimak, L., Giraud, Y., Metz, L., Yvorra, P. (Eds.), 2024a. Mandrin, des Derniers Néandertaliens aux Premiers Hommes Modernes en France Méditerranéenne. Artisanats et Territoires, Aix-en-Provence. In press.
Slimak, L., Zanolli, C., Muth, X., Metz, L., 2024b, In press. Se confronter à la découverte d'un corps néandertaliens, In: Slimak, L., Giraud, Y., Metz, L., Yvorra, P. (Eds.), Mandrin, des Derniers Néandertaliens aux Premiers Humains Modernes en France Méditerranéenne. Artisanats et Territoires, Aix-en-Provence, pp. 664–675.
Slimak, L., Vimala, T., Seguin-Orlando, A., Metz, L., Zanolli, C., Joannes-Boyau, R., Frouin, M., Arnold, L.J., Demuro, M., Devièse, T., Comeskey, D., Buckley, M., Camus, H., Muth, X., Lewis, J.E., Bocherens, H., Yvorra, P., Tenailleau, C., Duployer, B., Coqueugniot, H., Dutour, O., Higham, T., Sikora, M., 2024c, In press. Long genetic and social isolation in Neanderthals before their extinction. Cell Genom. 4, 100593.
Smith, B.H., 1984. Patterns of molar wear in hunter-gatherers and agriculturalists. Am. J. Phys. Anthropol. 63, 39–56.
Soressi, M., 2002. Le Moustérien de tradition acheuléenne du sud-France. Discussion sur la signification du faciès à partir de l'étude comparée de quatre sites: Pech-de-l'Azé I, Le Moustier, La Rochette et la Grotte XVI. Ph.D. Dissertation, Université Bordeaux 1.
Spencer, M.A., 2003. Tooth-root form and function in platyrrhine seedeaters. Am. J. Phys. Anthropol. 122, 325–335.
Tillier, A.M., Arensburg, B., Rak, Y., Vandermeersch, B., 1995. Middle Paleolithic dental caries: new evidence from Kebara (mount Carmel, Israel). J. Hum. Evol. 29, 189–192.
Trinkaus, E., 2018. An abundance of developmental anomalies and abnormalities in Pleistocene people. Proc. Natl. Acad. Sci. USA 115, 11941–11946.
Trinkaus, E., Maley, B., Buzhilova, A.P., 2008. Brief communication: Paleopathology of the Kiik-Koba 1 Neandertal. Am. J. Phys. Anthropol. 137, 106–112.
Turner II, C.G., Nichol, C.R., Scott, G.R., 1991. Scoring procedures for key morphological traits of the permanent dentition: the Arizona State University dental anthropology system. In: Kelley, M., Larsen, C. (Eds.), Advances in Dental Anthropology. Wiley-Liss, New York, pp. 13–31.
Vázquez Mosquerira, V.M., Espinosa Meléndez, M.T., Hernández Flores, F., 2018. Presence of the fourth molar. Literature review. Rev. Odont. Mex. 22, 103–117.
Voisin, J.-L., Condemi, S., Wolpoff, M.H., Frayer, D.W., 2012. A new online database. PaleoAnthropology 2012, 241–244. http://anthropologicaldata.free.fr) andashortreflectionabouttheproductiveuseofcompilingInternetdata.
Volpato, V., Macchiarelli, R., Guatelli-Steinberg, D., Fiore, L., Frayer, D.W., 2012. Hand to Mouth in a Neandertal: right-Handedness in Regourdou 1. PLoS One 7, e43949.
Wang, X.P., Fan, J., 2011. Molecular genetics of supernumerary tooth formation. Genesis 49, 261–277.
Zanolli, C., 2024. Les restes humains dentognathiques de Thorin. In: Slimak, L., Giraud, Y., Metz, L., Yvorra, P. (Eds.), Mandrin, des Derniers Néandertaliens aux Premiers Humains Modernes en France Méditerranéenne. Artisanats et Territoires, Aix-en-Provence, pp. 682–693. In press.
Zanolli, C., Pan, L., Dumoncel, J., Kullmer, O., Kundrát, M., Liu, W., Macchiarelli, R., Mancini, L., Schrenk, F., Tuniz, C., 2018. Inner tooth morphology of *Homo erectus* from Zhoukoudian. New evidence from an old collection housed at Uppsala University, Sweden. J. Hum. Evol. 116, 1–13.
Zanolli, C., Genochio, L., Tournepiche, J.-F., Mazurier, A., Macchiarelli, R., 2020. The Neanderthal mandible BD1 from Chaise-de Vouthon Abri Bourgeois–Delaunay (Charente, southwestern France, OIS 5E). PALEO 30, 346–359.
Zilhão, J., d'Errico, F. (Eds.), 2003. The Chronology of the Aurignacian and of the Transitional Technocomplexes. Dating, Stratigraphies, Cultural Implications. Instituto Portugues de Arqueologia, Lisbon.